Mouse liver repopulation with hepatocytes generated from human fibroblasts

Saiyong Zhu[1,*], **Milad Rezvani**[2,*], **Jack Harbell**[3,*], **Aras N. Mattis**[2,4,5], **Alan R. Wolfe**[6], **Leslie Z. Benet**[6], **Holger Willenbring**[2,3,4,#], and **Sheng Ding**[1,7,#]

[1]Gladstone Institute of Cardiovascular Disease, 1650 Owens Street, San Francisco, CA 94158, USA.

[2]Eli and Edythe Broad Center of Regeneration Medicine and Stem Cell Research, University of California San Francisco, 35 Medical Center Way, San Francisco, CA 94143, USA.

[3]Department of Surgery, Division of Transplantation, University of California San Francisco, 505 Parnassus Avenue, San Francisco, CA 94143, USA.

[4]Liver Center, University of California San Francisco, 1001 Potrero Avenue, San Francisco, CA 94110, USA.

[5]Department of Pathology, University of California San Francisco, 505 Parnassus Avenue, San Francisco, CA 94143, USA.

[6]Department of Bioengineering and Therapeutic Sciences, University of California San Francisco, 533 Parnassus Avenue, San Francisco, CA 94143, USA.

[7]Department of Pharmaceutical Chemistry, University of California San Francisco, 600 16th Street, San Francisco CA 94158, USA.

Abstract

Human induced pluripotent stem cells (iPSCs) promise to revolutionize research and therapy of liver diseases by providing a source of hepatocytes for autologous cell therapy and disease modeling. However, despite progress in advancing the differentiation of iPSCs into hepatocytes (iPSC-Heps) *in vitro*[1–3], cells that replicate the ability of human primary adult hepatocytes (aHeps) to proliferate extensively *in vivo* have not been reported. This deficiency has hampered

Corresponding author Correspondence should be addressed to Holger Willenbring (willenbringh@stemcell.ucsf.edu) or Sheng Ding (sheng.ding@gladstone.ucsf.edu).
*Joint first authors
#Joint senior authors
These authors contributed equally to this work.

efforts to recreate human liver diseases in mice, and has cast doubt on the potential of iPSC-Heps for liver cell therapy. The reason is that extensive post-transplant expansion is needed to establish and sustain a therapeutically effective liver cell mass in patients, a lesson learned from clinical trials of aHep transplantation[4]. As a solution to this problem, we report generation of human fibroblast-derived hepatocytes that can repopulate mouse livers. Unlike current protocols for deriving hepatocytes from human fibroblasts, ours did not generate iPSCs, but shortcut reprogramming to pluripotency to generate an induced multipotent progenitor cell (iMPC) state from which endoderm progenitor cells (iMPC-EPCs) and subsequently hepatocytes (iMPC-Heps) could be efficiently differentiated. For this, we identified small molecules that aided endoderm and hepatocyte differentiation without compromising proliferation. After transplantation into an immune-deficient mouse model of human liver failure, iMPC-Heps proliferated extensively and acquired levels of hepatocyte function similar to aHeps. Unfractionated iMPC-Heps did not form tumors, most likely because they never entered a pluripotent state. To our knowledge, this is the first demonstration of significant liver repopulation of mice with human hepatocytes generated *in vitro*, which removes a long-standing roadblock on the path to autologous liver cell therapy.

Current protocols for directed hepatocyte differentiation of iPSCs (or human embryonic stem cells; ESCs) produce cells that express many functions of aHeps[1–3]. Some functions of iPSC/ESC-Heps, e.g., CYP450 enzyme expression, are underdeveloped, whereas others, e.g., albumin (ALB) synthesis, are near normal. Therefore, human serum ALB (HSA) levels have been used to follow the fate and measure the expansion of iPSC/ESC-Heps transplanted into mice. Since the advent of protocols for hepatocyte differentiation of iPSCs/ESCs, numerous results from transplantation of these cells into mice have been reported. All of these studies, even those in which transplanted iPSC/ESC-Heps had a growth advantage, failed to reach HSA levels above 2 μg/mL[5–7], which is over 1,000-fold lower than what has been achieved with aHeps[8], and reflects less than 0.05% liver repopulation (data not shown). These disappointing results have been largely attributed to failure of iPSC/ESC-Hepsto proliferate after transplantation.

Reprogramming of somatic cells to a stable pluripotent state followed by differentiation into another cell type is a complicated process. Alternatively, the developmentally plastic state established soon after reprogramming factor overexpression can be harnessed for lineage conversion. Using this approach we and others previously induced human fibroblasts (Fibs) to assume a multipotent progenitor cell (iMPC) state that allowed efficient differentiation into myeloid[9] or smooth muscle and endothelial cells[10,11]. Because these iMPC derivatives could proliferate extensively, we reasoned that this method could be used to generate hepatocytes that were not compromised by growth arrest.

To investigate this possibility, we transduced 1×10^4 Fibs with retroviruses expressing OCT4, SOX2, and KLF4[12], and replated them for reprogramming into endoderm in medium containing established growth factors and the small molecule CHIR99021 (CHIR)[1–3] (Fig. 1). Only 14 days later, we detected expression of the endoderm-specific genes *SOX17* and *FOXA2* by quantitative reverse-transcription PCR (qRT-PCR) (Extended Data Fig. 1a). While only around 20 SOX17-and FOXA2-positive colonies formed under these conditions, exposing the cells to additional small molecules known to promote reprogramming[13,14]

increased the number of colonies to over 80 (Extended Data Fig. 1b–d and Supplementary Table 1).

Next, we investigated whether *de novo* endoderm differentiation was preceded by a pluripotent state. We found no expression of the pluripotency-specific genes *OCT4* and *NANOG* even at the earliest stages of the reprogramming process (Extended Data Fig. 1e). Because avoiding a pluripotent state decreases the cells' tumor risk, we confirmed this result by TRA-1-60[15] flow cytometry at the end of the reprogramming process (Extended Data Fig. 1f,g). In addition, we monitored cultures undergoing reprogramming for FOXA2-positive cells, referred to as iMPC-EPCs, and NANOG-positive cells by immunostaining and flow cytometry (Extended Data Fig. 2a). We found FOXA2-positive cells already 16 days after initiating reprogramming, whereas NANOG-positive cells were always absent (Extended Data Fig. 2b–d). We also used doxycycline (Dox)-inducible lentiviruses expressing OCT4, SOX2, and KLF4 to compare the dynamics of reprogramming to endoderm versus pluripotency (Extended Data Fig. 3a). We detected iMPC-EPC colonies in transduced cultures grown under iMPC-EPC reprogramming conditions for 21 days after only 7 days of Dox treatment. In contrast, generating iPSCs required treating the cultures with Dox for 14 days and growing them under iPSC reprogramming conditions for 30 days (Extended Data Fig. 3b). Our findings that Fibs reprogram into iMPC-EPCs faster than into iPSCs and without expressing pluripotency markers show that our protocol does not produce a pluripotent intermediate stage, which confirms previous results from shortcutting reprogramming to pluripotency for lineage conversion[9–11].

We also determined whether iMPC-EPCs could be expanded *in vitro*, a prerequisite for producing the large quantities needed for human liver cell therapy. We found that combining CHIR with A83-01 (A83)[16] increased iMPC-EPC colony size (Fig.1 and Extended Data Fig. 4a). Adding EGF and bFGF caused further expansion and facilitated pass aging for more than 25 times, producing more than 1×10^{16} iMPC-EPCs from a single colony (Fig. 2a,b, Extended Data Fig.4b, and Supplementary Table 1). These cells exhibited high viability after cryopreservation (data not shown).

Importantly, expanding iMPC-EPCs maintained endoderm differentiation, as evidenced by positive SOX17 and FOXA2 immunostaining and negative NANOG immunostaining (Fig. 2a and Extended Data Fig. 4c). Expanding iMPC-EPCs acquired HNF4α expression (Fig. 2a and Extended Data Fig. 4d), suggesting further specification. To define their stage of differentiation, we compared iMPC-EPCs to ESC-derived definitive endoderm cells (DECs) and primitive gut-tube endoderm cells (GECs)[17] (Fig. 2c). We found that iMPC-EPCs resembled ESC-GECs, except for lack of *OCT4* and *NANOG* expression. iMPC-EPCs also lacked expression of the ectoderm- and mesoderm-specific genes *PAX6* and *BRY*, suggesting commitment to endoderm differentiation. Further analyses showed that iMPC-EPCs had a propensity for differentiating into liver and pancreas, but not lung or intestine (Extended Data Fig. 4e,f and data not shown). These results establish the feasibility of generating from Fibs endoderm cells that share many characteristics with previously reported ESC/iPSC-derived endodermal progenitor cell lines[18], but appear more lineage restricted and never entered a pluripotent state.

To further differentiate iMPC-EPCs into iMPC-Heps, we cultured them in medium containing factors reported to drive hepatic differentiation of iPSC-DECs[1,3] (Fig. 1). These factors were effective in inducing expression of the fetal hepatocyte marker α-fetoprotein (AFP), but few cells expressed the more mature markers ALB and α-1 Antitrypsin (AAT) (Extended Data Fig. 5a). To improve hepatocyte differentiation, we screened small molecules for inducers of *ALB* gene expression, of which A83 and the Notch inhibitor Compound E (C–E)[16] were effective (Extended Data Fig.5b). Because TGFβ and Notch signaling direct bipotential embryonic liver progenitor cells toward biliary fate[19,20], our results suggest that inhibiting biliary differentiation promotes hepatocyte differentiation.

Like aHeps, iMPC-Heps had a polygonal shape, were occasionally binucleated, and expressed the hepatocyte markers HNF4α, ALB, AAT, and cytokeratin 18 (CK18) (Fig. 3a). iMPC-Heps also exhibited hepatocyte functions like glycogen storage, lipid uptake and storage, and urea production (Extended Data Fig.6a,b). Gene expression analysis showed that iMPC-Heps generally resembled human primary fetal hepatocytes (fHeps)(Fig. 3b), although some cells were less differentiated (Fig. 3c and Supplementary Table 1). Analysis of ALB secretion and CYP450 activities confirmed that iMPC-Heps were less mature than aHeps, but also showed that iMPC-Heps were more differentiated than iPSC-Heps generated as previously reported[1,3] (Fig. 3d,e and Extended Data Fig. 6c). The media used for iMPC-EPC/Hep generation did not produce iPSC-Heps with improved function, which underscores the importance of reprogramming-induced developmental plasticity in this process (Extended Data Fig. 6d).

To test whether iMPC-Heps can expand after transplantation, we transplanted 1×10^6 cells into FRG mice, an immune-deficient mouse model of human tyrosinemia type I[8]. The liver injury caused by this disease creates a growth advantage for differentiated hepatocytes, but not immature liver progenitor cells. Therefore, liver repopulation of FRG mice requires both mature hepatocyte function and ability to proliferate. To detect expansion of the transplanted iMPC-Heps, we measured HSA levels monthly for more than 9 months. The earliest we could detect HSA was 2 months after transplantation (Fig. 4a), when levels were at most 140 ng/mL, but they increased continuously, reaching levels of up to 104 μg/mL 6 months later. By this time, HSA levels were 10-fold higher in control FRG mice transplanted with 1×10^6 aHeps. The delayed onset but parallel upward trend of HSA levels in iMPC-Hep-transplanted mice, as compared to control mice, suggested that iMPC-Heps were inferior to aHeps in engraftment efficiency, and the need for post-transplant maturation, but not in the ability to proliferate. Indeed, we found that although iMPC-Heps generated significantly fewer repopulating nodules than aHeps (data not shown), these nodules grew markedly between 3 and 9 months after transplantation (Extended Data Fig. 7a). Moreover, iMPC-Heps still proliferated 9 months after transplantation (Fig. 4b). To date, we have observed a maximum nodule size of 4,000 iMPC-Heps and a liver repopulation level of 2% (Extended Data Fig. 7b,c).

To determine whether iMPC-Heps matured after transplantation, we compared the global gene expression profiles of transplanted iMPC-Heps and aHeps. For this, we isolated nodules of iMPC-Heps and aHeps by laser-capture microscopy (LCM) (Extended Data Fig. 7d,e), and analyzed their RNA with microarrays. We found that iMPC-Heps and aHeps

clustered closely together—very few genes were differentially expressed, none of which were of known importance for hepatocyte function (Fig. 4c, Extended Data Fig. 8a–e, and Supplementary Table 2). We also compared cultured iMPC-Heps and freshly isolated aHeps. We found marked differences in gene expression between these two cell types, which illustrates the extensive maturation iMPC-Heps underwent after transplantation. In fact, before transplantation, the gene expression profile of iMPC-Heps resembled that of iPSC-Heps. We confirmed the microarray results by qRT-PCR and immunostaining (Fig. 4d and Extended Data Fig. 9a–c). In addition, we determined whether maturation of gene expression translated into normal function by measuring debrisoquine (DB) hydroxylation— a unique function of human hepatocytes executed by CYP2D6[21]—in mice repopulated to similar levels with iMPC-Heps or aHeps. We found no difference in plasma 4-hydroxy-debrisoquine (4-OH-DB) levels between these mice, which shows that CYP2D6 matured in iMPC-Heps from negligible expression levels *in vitro* to normal activity*in vivo*(Figs 4e and 3b). In accord with a need for post-transplant maturation of iMPC-Heps, which is reminiscent of iPSC/ESC-derived pancreatic β-cells[22], we found that iMPC-Hep transplantation improved survival of mice with chronic liver failure, but not acute liver failure (Extended Data Fig. 10a,b).

Finally, we ruled out fusion with mouse hepatocytes as the reason for post-transplant maturation and proliferation of iMPC-Heps (Fig. 4f), and investigated the origin of dysplastic nodules observed in some iMPC-Hep and aHep recipients (Extended Data Fig. 10c). Absence of differentiation-independent, human-specific β2-microglobulin expression showed that these nodules originated from mouse cells, thus representing a known complication of tyrosinemia type I (Extended Data Fig.10d)[23].

Our results show that iMPC-Heps are not impacted by limitations of iPSC/ESC-Heps generated with current protocols, particularly deficiencies in *in vivo* efficacy and safety. While many aspects of iMPC-Hep generation and transplantation remain to be explored and improved, the fact that these cells can fully mature and proliferate for months after transplantation establishes them as promising candidates for *in vivo* modeling and autologous therapy of human liver diseases.

METHODS

Generation of iMPC-EPCs from Fibs

Human newborn fibroblasts (CRL-2097, ATCC) were cultured in a 10-cm tissue culture dish coated with 0.1% gelatin, and transduced twice with freshly produced retrovirus supernatants as previously described[12,24]. For reprogramming, 1×10^4 transduced cells were seeded in a 10-cm tissue culture dish coated with 0.1% gelatin, and cultured in reprogramming initiation medium (RIM) supplemented with 3 μM CHIR, 100 μM DLPC (Tocris), 0.1 mM NaB, 2 μM Par, 0.5 μM RG, 10 ng/mL EGF, and 10 ng/mL bFGF for 7 days, followed by culture in endoderm differentiation medium (EDM) supplemented with 3 μM CHIR, 100 μM DLPC, 0.1 mM NaB, 2 μM Par, 0.5 μM RG, and 100 ng/mL Activin A for 14–21 days. Reprogrammed colonies were picked at day 21–28 for expansion on passage 4 irradiated CF1 mouse embryonic fibroblasts (MEFs) in endoderm expansion medium (EEM) supplemented with 3 μM CHIR, 10 ng/mL EGF, 10 ng/mL bFGF, and 0.5 μM A83,

and were passaged at a ratio of 1:4–1:6 after dissociation with Accutase. To prevent cell death, 0.5 μM thiazovivin was added to the medium in the first 12–24 hours after each passage. RIM: DMEM/F12, 10% Knockout Serum Replacement (KSR), 5% ES-FBS, 1% Glutamax, 1% Non-Essential Amino Acids (NEAA), 1% Penicillin/Streptomycin (P/S), and 0.1 mM β-mercaptoethanol (β-ME). EDM: Advanced RPMI, 2% ES-FBS, 1% Glutamax, 1% NEAA, 1% P/S, and 0.1 mM β-ME. EEM: DMEM, 1% Glutamax, 0.5×N2, 0.5×B27 (without vitamin A), 5 μg/mL BSA, and 1% P/S. All cell culture reagents were from Invitrogen and all chemicals and all growth factors were from Stemgent except where otherwise specified.

Generation of iMPC-Heps from iMPC-EPCs

The principles of the protocol were adopted from previously published protocols[1,25], modified, and improved by the addition of small molecules. Briefly, iMPC-EPCs were cultured in EEM for 4–5 days, in hepatocyte differentiation medium (HDM) supplemented with 20 ng/mL bFGF, 20 ng/mL BMP4 (Stemgent), 0.1 μM Dex (Sigma-Aldrich), and 0.5 μM A83 (Stemgent) for 4 days, and finally in hepatocyte maturation medium (HMM), consisting of HCM (Hepatocyte Culture Medium, Lonza) supplemented with 0.5 μM A83, 0.1 μM Dex, 20 ng/mL HGF (R&D), 20 ng/mL OSM (R&D), and 0.1 μM C–E (EMD Millipore), for 7–10 days. iMPC-Heps were passaged at a ratio of 1:4 using Accutase, and cultured in HCM until use for analysis or transplantation. HDM: DMEM, 1% Glutamax, 1×B27, and 1% P/S.

Generation of DECs and GECs from ESCs

H9 ESCs (WiCell WA09) were cultured on matrigel (BD; 1:50 dilution)-coated 6-well plates with Essential 8 Medium (Invitrogen) for 3 days. For endoderm differentiation, cells were cultured in RPMI 1640, 1% Glutamax, 1% P/S, 100 ng/mL Activin A, and 3 μM CHIR for 1 day, RPMI 1640, 1% Glutamax, 0.2% ES-FBS, 1% P/S, and 100 ng/mL Activin A for 2 days, followed by DMEM/F12, 1% Glutamax, 2% ES-FBS, 1% P/S, 25 ng/mL FGF7 (R&D), and 25 ng/mL FGF10 (R&D) for 3 days. As previously reported[17], cell populations at day 3 and day 6 of differentiation were considered ESC-DECs and ESC-GECs, respectively.

Generation of iPSC-Heps

Normal donor iPSCs grown on passage 3 irradiated CF1 MEFs were differentiated into DECs for 5–7 days as previously described[3] using insulin-free B27 (Invitrogen) instead of FBS. DECs were differentiated directly (without splitting) into iPSC-Heps by culture in IMDM (Invitrogen) containing B27 with insulin (Invitrogen), 1% Glutamax, 0.3 mM monothioglycerol (Sigma-Aldrich), 1% Antibiotic-Antimycotic (Invitrogen), 0.126 U/mL human insulin (Sigma-Aldrich), 10 ng/mL bFGF, 20 ng/mL BMP4, and 100 nM Dex for 5 days. Maturation was continued using the same medium additionally supplemented with 20 ng/mL HGF for 15–20 days before switching to HCM supplemented with 20 ng/mL HGF and 20 ng/mL OSM for 5–7 days similar to previously reported protocols[1,3]. All growth factors were purchased from R&D. Differentiation was performed entirely at 37°C in 5% O2/5% CO2 with daily media changes.

Reprogramming using temporally controlled transcription factor overexpression

Dox-inducible lentiviruses carrying the reprogramming factors OCT4, SOX2, and KLF4 were previously described[26]. CRL-2097 fibroblasts were cultured in a 10-cm tissue culture dish coated with 0.1 % gelatin, and transduced twice with freshly produced lentivirus supernatants as previously described[13]. For iMPC-EPC reprogramming, 1×10^4 transduced cells were seeded in a 10-cm tissue culture dish coated with 0.1 % gelatin, and cultured in RIM supplemented with 4 μg/ml Dox, 3 μM CHIR, 100 μM DLPC, 0.1 mM NaB, 2 μM Par, and 0.5 μM RG for 7 days, 10 days, or 14 days, followed by culture in EDM supplemented with 3 μM CHIR, 100 μM DLPC, 0.1 mM NaB, 2 μM Par, 0.5 μM RG, and 100 ng/mL Activin A for 14 days, 11 days, or 7 days, respectively. For iPSC reprogramming, 1×10^4 transduced cells were seeded in a 10-cm tissue culture dish, and cultured in RIM supplemented with 4 μg/ml Dox, 3 μM CHIR, 100 μM DLPC, 0.1 mM NaB, 2 μM Par, and 0.5 μM RG for 7 days, 10 days, or 14 days, followed by treatment with iPSC medium (iPSCM) for 23 days, 20 days, or 16 days, respectively. iPSCM: DMEM/F12, 1% Glutamax, 20% KSR, 1% NEAA, 1% P/S, 0.1 mM β-ME, and 10 ng/mL bFGF.

Generation of iPSC-Heps with the iMPC-EPC/Hep generation protocol

Normal donor iPSCs were grown on passage 4 irradiated CF1 MEFs in iPSC medium for 3 days, and then treated with EDM supplemented with 3 μM CHIR, 100 μM DLPC, 0.1 mM NaB, 2 μM Par, and 0.5 μM RG, and 100 ng/mL Activin A for 2 weeks. After Accutase dissociation, the resulting cells were passaged at a ratio of 1:4 onto irradiated CF1 MEFs and cultured in EEM for 4 days. Next, the cells were cultured in HDM supplemented with 20 ng/mL bFGF, 20 ng/mL BMP4, 0.1 μM Dex, and 0.5 μM A83 for 4 days, and finally in HMM, consisting of HCM supplemented with 0.5 μM A83, 0.1 μM Dex, 20 ng/mL HGF, 20 ng/mL OSM, and 0.1 μM C–E, for another 10 days.

Cell immunostaining

Standard immunostaining was carried out as previously reported[13]. Primary antibodies were goat anti-SOX17 antibody (R&D, Cat # AF1924) diluted 1: 1,000, rabbit anti-FOXA2 antibody (Millipore, Cat # AB4125) diluted 1:500, goat anti-FOXA2 antibody (R&D, Cat # AF2400) diluted 1:1,000, mouse anti-HNF4α antibody (Perseus Proteomics, Cat # PP-H1415-00) diluted 1:500, mouse anti-AAT antibody (Thermo Scientific, Cat # MA190438) diluted 1:500, goat anti-PDX1 antibody (R&D, Cat # AF2419) diluted 1:1,000, goat anti-OCT4 antibody (Santa Cruz Biotechnology, Cat # sc-8629) diluted 1:500, rabbit anti-NANOG antibody (Abcam, Cat # ab80892) diluted 1:500, mouse anti-AFP antibody (Sigma-Aldrich, Cat # A8452) diluted 1:500, mouse anti-CK18 antibody (Abcam, Cat # ab82254) diluted 1:500, and goat anti-albumin antibody (Bethyl, Cat # A80-129A) diluted 1:500. Secondary antibodies were Alexa Fluor 488/555 donkey anti-mouse or anti-rabbit or anti-goat IgG (1:1,000) (Invitrogen). Nuclei were visualized by Hoechst (Sigma-Aldrich) staining. Images were captured using a Nikon Eclipse TE2000-U microscope.

Flow cytometry

Cells were harvested by Accutase dissociation at 37°C for 2–5 minutes, and fixed with 4% formaldehyde in D-PBS (Sigma-Aldrich) on ice for 10 minutes. Afterwards, cells were

washed 5 times with ice-cold Perm/Wash buffer (BD). To remove undissociated cell clusters, cells were passed twice through 70-μm cell strainers (BD). Cells were immunostained with goat anti-FOXA2 antibody (R&D, Cat # AF2400) diluted 1:100, rabbit anti-NANOG antibody (Abcam, Cat # ab80892) diluted 1:20, mouse anti-HNF4α antibody (Perseus Proteomics, Cat # PP-H1415-00) diluted 1:100, goat anti-human albumin antibody (Bethyl, Cat # A80-129A) diluted 1:100, mouse anti-CK18 antibody (Abcam, Cat # ab82254) diluted 1:100, or PE-conjugated mouse anti-TRA-1-60 antibody (Biolegend, Cat #330609) diluted 1:50 on ice for 2 hours. To determine background levels of each immunostaining, cell aliquots were incubated with the respective isotype control antibodies. After immunostaining, cells were washed 5 times with Perm/Wash buffer. Cells were then incubated individually with Alexa Fluor 488-conjugated or Alexa Fluor 555-conjugated antibodies (Invitrogen) diluted 1:500 on ice for 1 hour. Afterwards, cells were washed 5 times with Perm/Wash buffer. Finally, cells were resuspended in 0.5 mL ice-cold D-PBS supplemented with 2% FBS, and flow cytometry was performed on a FACSCalibur system using CellQuest software (BD). FlowJo software (Tree Star) was used to analyze the data.

qRT-PCR

Total RNA was extracted using the miRNeasy Mini Kit (Qiagen) or RNeasy Plus Mini Kit in combination with QIAshredder (Qiagen). First-strand reverse transcription was performed with 0.5–1 μg RNA using the iScript cDNA Synthesis Kit (BioRad) or qScript cDNA Supermix (Quanta Biosciences). qRT-PCR was performed using PerfeCTa SYBR Green SuperMix (Quanta) or iQ SYBR Green Supermix (Bio-Rad) on an Applied Biosciences ViiA 7 Real-Time PCR System (Invitrogen). aHeps purchased from Yecuris or the Liver Tissue Cell Distribution System (NIH) and fHeps obtained from StemExpress were shipped overnight in suspension, centrifuged for 5 minutes at $300 \times g$ immediately after arrival, and stored as cell pellets at −80°C prior to RNA extraction. Primer sequences are shown in Supplementary Table 3. Human gene-specific primers were derived from previous publications[8,27–33].

CYP450 activity analysis

Luminescence-based P450-Glo Assays (Promega) were used to measure the activities of the CYP3A family (Luciferin-PFBE, Cat # V8901), CYP3A4 (Luciferin-IPA, Cat # V9001), and CYP2C19 (Luciferin-H EGE, Cat # V8881) following the manufacturer's instructions. Results are shown as Luminescent Counting Units (LCU)/minute normalized to a million viable cells. Cell viability was assessed by Trypan Blue Stain (Invitrogen). Metabolically well-characterized aHeps (Life Technologies HMCPMS Lot# Hu8138) were used as positive controls.

PAS staining

PAS (Sigma-Aldrich) staining was performed following the manufacturer's instructions.

Lipid staining

BODIPY 493/503 (Life Technologies) solution (1 mg/mL) was added to the medium (2 μL per well of a 12-well plate); 1 hour later, the cells were washed with medium, and imaged

using fluorescence microscopy. For ORO staining, cells were fixed in 10% formalin, incubated with ORO staining solution (Sigma-Aldrich) for 1 hour at room temperature, washed with water, and imaged using light microscopy.

LDL uptake assay

Dil-ac-LDL (Invitrogen) was added to the medium (5 μL per well of a 12-well plate); 2 hours later, the cells were washed with medium, and imaged using fluorescence microscopy.

Urea production

Cell culture supernatant was collected and analyzed using the QuantiChrom Urea Assay Kit (BioAssay Systems) following the manufacturer's instructions.

ALB ELISA of cell culture supernatants

The amount of ALB in cell culture supernatants was determined using a human-specific albumin ELISA kit (Assaypro, Cat # EA3201-1) following the manufacturer's instructions. Cells were cultured in HMM for 24 hours, and the supernatant was collected for analysis. Control aHeps (Life Technologies HMCPMS Lot # Hu8138) were analyzed 24 hours after plating.

Mice and transplantation

Procedures involving mice were approved by the Institutional Animal Care Committee at the University of California San Francisco. Immune-deficient, fumarylacetoacetate hydrolase (Fah)-deficient mice lacking B, T, and natural killer cells due to disruption of *Rag2* and *Il2rg*–so-called FRG mice–were used as recipients[8]. Mice were maintained on NTBC (Yecuris) in the drinking water at 16 mg/L. 1 day before transplantation, mice were taken off NTBC. An adenovirus expressing urokinase plasminogen activator (Ad-uPA) was used for liver preconditioning[34]. Ad-uPA was delivered by retroorbital injection 24 hours before transplantation at a dose of 5×10^7 PFU/g body weight. Transplantation was performed by intrasplenic injection through a left flank incision under isoflurane anesthesia and buprenorphine analgesia. After transplantation, mice received NTBC in the drinking water in cycles consisting of 7–10 days off NTBC and 2–3 days on NTBC at 4 mg/L. For surgical prophylaxis, 5 mg Naxcel (Pfizer) were given by intraperitoneal injection immediately before transplantation, and daily for 7 days. Due to the immune deficiency of the mice, all mice received prophylactic antibiotic treatment with Ciprofloxacin (Hospira) at 0.25 mg/mL in the drinking water for 7 days, then trimethoprim/sulfamethoxazole (TMP/SMX, Sigma-Aldrich) in the drinking water at 0.2 g/L TMP and 1 g/L SMX continuously. aHeps for transplantation were purchased from Yecuris, shipped overnight in suspension, and transplanted into recipient mice immediately after arrival.

HSA ELISA

HSA levels were determined using the Human Albumin ELISA Quantitation Set (Bethyl, Cat # E80-129). Blood (3 μL) drawn by tail clipping was immediately diluted 1:100 in sample diluent and HSA concentration was determined by ELISA using a human albumin-specific antibody.

Tissue immunostaining

Liver tissue harvested from recipient mice was frozen immediately in optimum cutting temperature (OCT) compound (Tissue-Tek, Sakura Finetek), or fixed in 4% paraformaldehyde (Sigma-Aldrich) or 10% formalin (Sigma-Aldrich) at 4°C overnight. Tissues for frozen sections were cryoprotected in 30% sucrose (Sigma-Aldrich) before embedding and freezing in OCT. Paraffin-embedded tissues were preserved in 70% ethanol prior to tissue processing and paraffin embedding. Frozen tissues were cut using a Leica 3050S Cryostat into 5–7 μm sections, air dried, and stored at −20°C prior to staining. Tissue sections were stained with rabbit anti-FAH antibody (gift from Robert Tanguay, Université Laval) diluted 1:15,000[35], mouse anti-Ki67 antibody (BD Pharmingen, Cat # 550609) diluted 1:25, FITC-conjugated goat anti-mouse albumin antibody (Bethyl, Cat # A90-234F) diluted 1:100, goat anti-human albumin antibody (Bethyl, Cat # A80-229A) diluted 1:100, rabbit anti-CYP2D6 antibody (Sigma-Aldrich, Cat # AV41675) diluted 1:200, rabbit anti-CYP3A4 antibody (Abcam, Cat # ab135813) diluted 1:50, or FITC-conjugated mouse anti-human β2-microglobulin antibody (BioLegend, Cat # 316304) diluted 1:200. Antigen retrieval with Citra solution (Biogenex) was done before immunostaining for Ki67 and mouse albumin. For co-immunostaining with anti-mouse and anti-human albumin antibodies, sections from unfixed OCT-embedded frozen tissue were fixed in 100% ethanol[36]. For fluorescence microscopy, primary antibodies were detected with donkey anti-rabbit conjugated with Cy3 (Jackson ImmunoResearch), donkey anti-goat conjugated with Alexa Fluor 488 (Jackson ImmunoResearch), donkey anti-goat conjugated with Alexa Fluor 594 (Jackson ImmunoResearch), donkey anti-rabbit conjugated with Alexa Fluor 488 (Invitrogen), or the M.O.M. Fluorescein kit (Vector). Nuclear DNA was stained with 2 μg/mL DAPI (Invitrogen).

Quantification of liver repopulation

Overall liver repopulation with transplanted iMPC-Heps was determined by measuring the area of recipient mouse liver sections composed of iMPC-Heps by ALB and FAH immunostaining relative to the total area of liver tissue. Sections were taken from 6 separate pieces of liver tissue from different parts of the recipient's liver. Areas were calculated using ImageJ software (NIH). The number of iMPC-Heps per nodule was estimated using a previously described method[35,37]. Briefly, the number of iMPC-Heps present in the 2-dimensional section showing the widest diameter of a repopulating nodule was multiplied by a previously determined correction factor to estimate the total number of hepatocytes comprising the 3-dimensional nodule.

LCM and microarray analysis

Repopulating nodules were isolated using a PALM MicroBeam IV system (Zeiss) around 9 months after transplantation. PALM RoboSoftware 4.3 SP1 was used to create LCM matrices based on ALB immunostaining of cryosections flanking a 7 μm unfixed cryosection from which nodules were isolated. Multiple nodules from a mouse were pooled to generate a sample. RNA was extracted and purified using the Arcturus Pico Pure RNA Isolation Kit (AB Biosystems). RNA quality was analyzed using chip-based capillary electrophoresis (Bioanalyzer, Agilent), and quantity and purity were determined with a

NanoDrop spectrometer. The NuGEN Pico V2 kit was used for amplification, fragmentation, and biotin labeling. Labeled cDNA was hybridized to GeneChip Human Gene 1.0 ST Arrays (Affymetrix). Signal intensity fluorescent images produced during Affymetrix GeneChip hybridizations were read using the Affymetrix Model 3000 Scanner and converted into GeneChip probe results files (CEL) using Command and Expression Console software (Affymetrix). Results were deposited in Gene Expression Omnibus (accession # GSE52309). Arrays were normalized for array-specific effects using Affymetrix Robust Multi-Array (RMA) normalization. Normalized array values were reported on a log2 scale. For statistical analyses, background noise was eliminated by removing probesets for which no experimental group had an average log2 intensity > 3. Linear models were fitted for each gene using Bioconductor limma in R. Moderated t statistics, fold change, and the associated P values were calculated for each gene. Heatmaps were created using heatmap.2 in R v2.11.0. Gene sets of hepatocyte function-related GO terms were obtained from MSigDB (http://www.broadinstitute.org/gsea/msigdb).

In vivo CYP2D6 activity analysis

Plasma samples (40 μL) were obtained by retroorbital blood draw at 0, 1 and 2 hours after administering 2 mg/kg body weight debrisoquine (DB; Enzo Life Sciences) in water by gavage. A standard curve was created by serial dilution of a solution with equal amounts of DB and 4-hydroxy-DB (Santa Cruz Biotechnology), using a 1:1 acetonitrile:H_2O solvent mixture. Aliquots of standard solutions not exceeding 5 μL in size were added to 100 μL of Swiss Webster K_2EDTA mouse plasma (Bioreclamation) to create plasma standards with concentrations from 0.01 μM to 50 μM. All plasma samples were precipitated with 4 volumes of cold acetonitrile, vortexed for 1 minute, and after standing for 30 minutes at −20°C, centrifuged for 5 minutes at $13,000 \times g$. The supernatants separated into upper and lower phases; the smaller lower phases were used in the analyses. DB and 4-OH-DB were measured by LC-MS/MS with an API4000 MS/MS mass spectrometer (AB Sciex) with ESI in the positive ion mode. They were detected using the transitions $176.1 \rightarrow 134.1$ and $192.1 \rightarrow 132.1$ m/z. Instrumental settings were 46 and 41 v for DP, and 25 and 27 v for CE, respectively. Settings in common for both analytes were CXP = 8 v, EP = 10 v, CAD = 12 v, IS = 5500 v, temp. = 600°C, CUR = 35 and GS1 = GS2 = 50. The LC method employed a 50×4.6 mm C18, 5 μm, 100 Å, Kinetex column (Phenomenex) and a binary mobile phase with A = 15% methanol:H_2O (with 160 mg/L $NH_4CH_3CO_2$, 0.1% formic acid, and 0.1% acetonitrile) and B = 100% methanol (with the same additions). Flow rate was 0.5 mL/minute. The gradient used was as follows: 0–1 minute, 0% B; 1–4 minutes, linear ramp to 100% B; 4–5 minutes, 100% B; 5 to 5.5 minutes, linear ramp to 0% B; 5.5 to 8.0 minutes, 0% B. Injection size was 3 μL, and retentions were 2.94 minutes for 4-OH-DB and 3.85 minutes for DB.

Survival studies

To model acute liver failure, FRG mice were taken off NTBC and injected with 5×10^7 PFU/g body weight Ad-uPA 1 day before transplantation. Mice were kept off NTBC and survival was recorded daily. To model chronic liver failure, mice were also taken off NTBC and injected with 5×10^7 PFU/g body weight Ad-uPA 1 day before transplantation, but NTBC was reinstated at a dose of 4 mg/L 7 days after transplantation. From there on, mice

were subjected to repeated cycles of NTBC off for 10 days and NTBC on for 3 days. Survival was recorded twice a week. For both liver failure models, 8–12-week-old FRG mice were used. Littermates were distributed between experimental and control groups. Male and female mice were equally distributed between groups. Blinding was not done. All transplanted mice were included in the analysis with the exception of mice that died within 24 hours after transplantation, which was considered a complication of the surgery, because Fah deficiency is known to take longer to unfold[35].

Statistical analysis

The standard deviation (SD) and standard error of the mean (SEM) were calculated from the average of at least 3 independent samples unless otherwise specified. Data were compared between experimental and control groups using Student's *t* test (unpaired, two-tailed). Survival was compared using the Mantel-Cox log-rank test. A *P* value of less than 0.05 was considered significant.

Extended Data
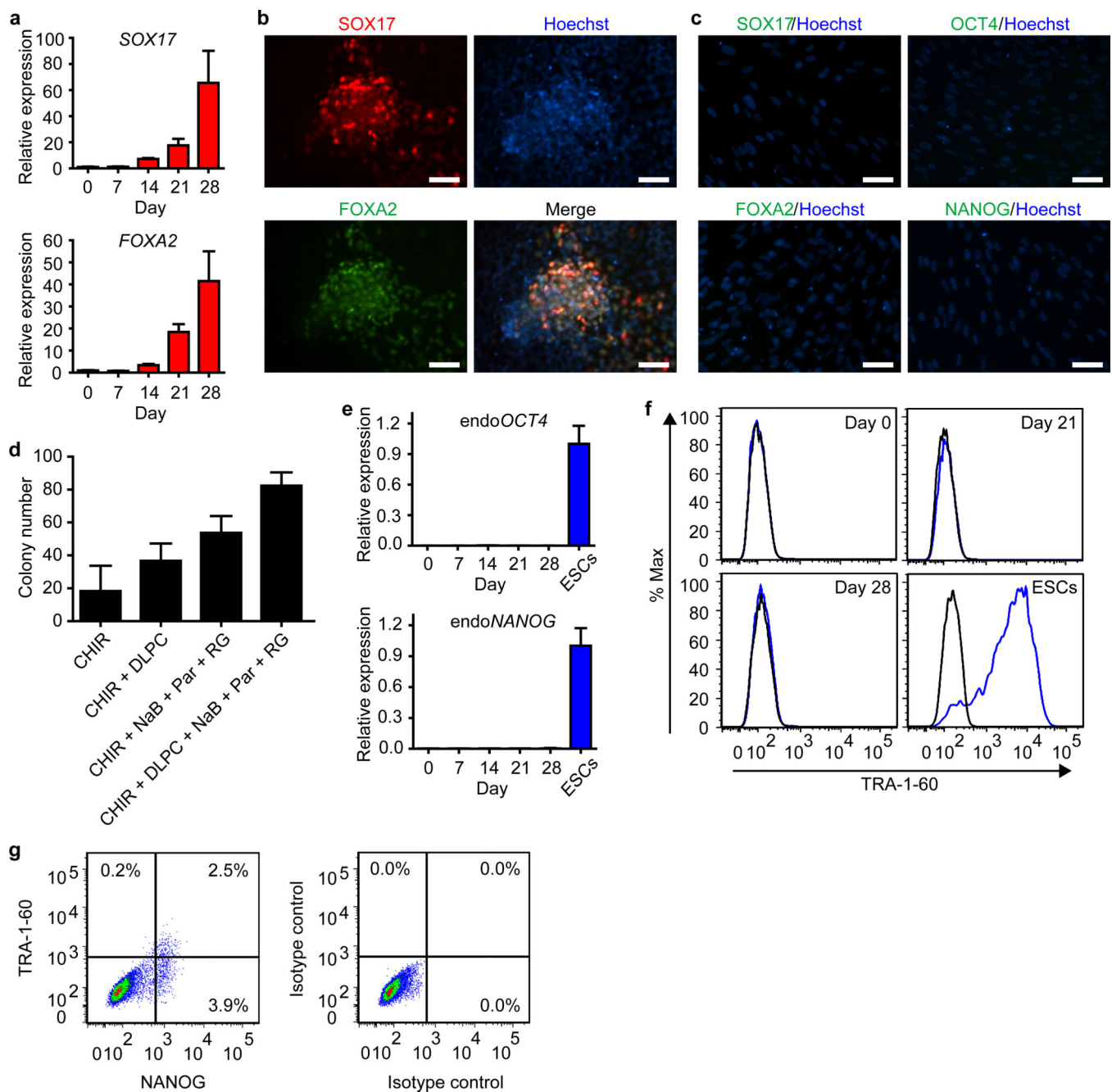
Extended Data Figure 1. Reprogramming of Fibs into endoderm progenitor cells without activation of pluripotency markers

a, qRT-PCR shows expression levels of the endoderm-specific genes *SOX17* and *FOXA2* during the reprogramming process (combination of initiation and reprogramming steps of the protocol) relative to starting cells at day 0. Error bars represent SEM of biological replicates (n = 3). **b,** Immunostainings show co-expression of SOX17 and FOXA2 in colonies at day 28. Scale bars = 100 μm. **c,** Immunostainings show absence of SOX17 and

FOXA2 and the pluripotency-specific markers OCT4 and NANOG in Fibs. Scale bars = 100 μm. **d,** Small molecules increase the number of colonies positive in FOXA2 immunostaining at day 28. Medium containing Activin A was additionally supplemented with the indicated small molecules. Error bars represent SEM of biological replicates (n = 3). **e,** qRT-PCR shows absence of endogenous (endo) *OCT4* and *NANOG* gene expression during reprogramming to endoderm. Gene expression levels are shown relative to ESCs. Error bars represent SEM of biological replicates (n = 3). **f,** Flow cytometry shows absence of cells expressing the pluripotency marker TRA-1-60 at the end of the reprogramming process. Cells at day 0 and ESCs were used as controls. At least 10,000 events were collected. **g,** Flow cytometry for TRA-1-60 and NANOG of 10,000 cells from a culture of Fibs transduced with retroviruses expressing OCT4, SOX2, and KLF4 and grown under iPSC reprogramming conditions for 30 days shows that both markers are effective in delineating rare cells reprogrammed to pluripotency. Because the number of NANOG-positive cells is higher than the number of TRA-1-60-positive cells, and virtually all TRA-1-60-positive cells are NANOG positive, NANOG appears to be a more sensitive marker in this process.
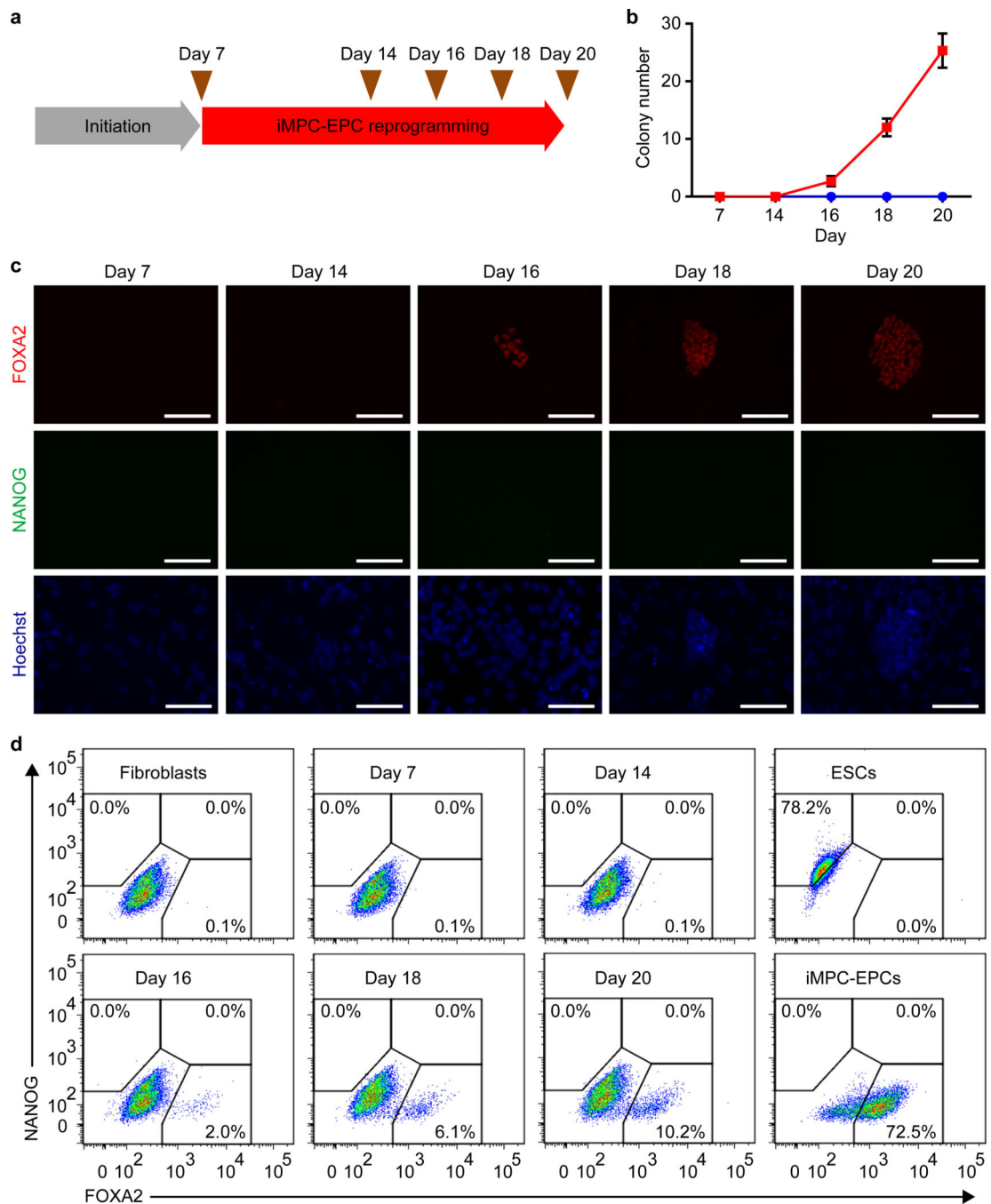
Extended Data Figure 2. Analysis of FOXA2 and NANOG expression at the colony and single-cell level during Fib-to-iMPC-EPC reprogramming

a, Schematic showing time points of analysis. **b,** Quantification of FOXA2-positive and NANOG-positive colonies forming during the reprogramming process. Error bars represent SEM of biological replicates (n = 3). **c,** Representative immunostainings show FOXA2-positive colonies emerging at day 16 of the reprogramming process and absence of NANOG-positive colonies or cells at all time points. Scale bars = 100 μm. **d,** Flow cytometry shows a gradual increase in the number of FOXA2-positive cells beginning at day

16 of the reprogramming process, whereas NANOG-positive cells are absent at all time points. Fibs, ESCs, and iMPC-EPCs were used as controls. At least 10,000 events were collected.
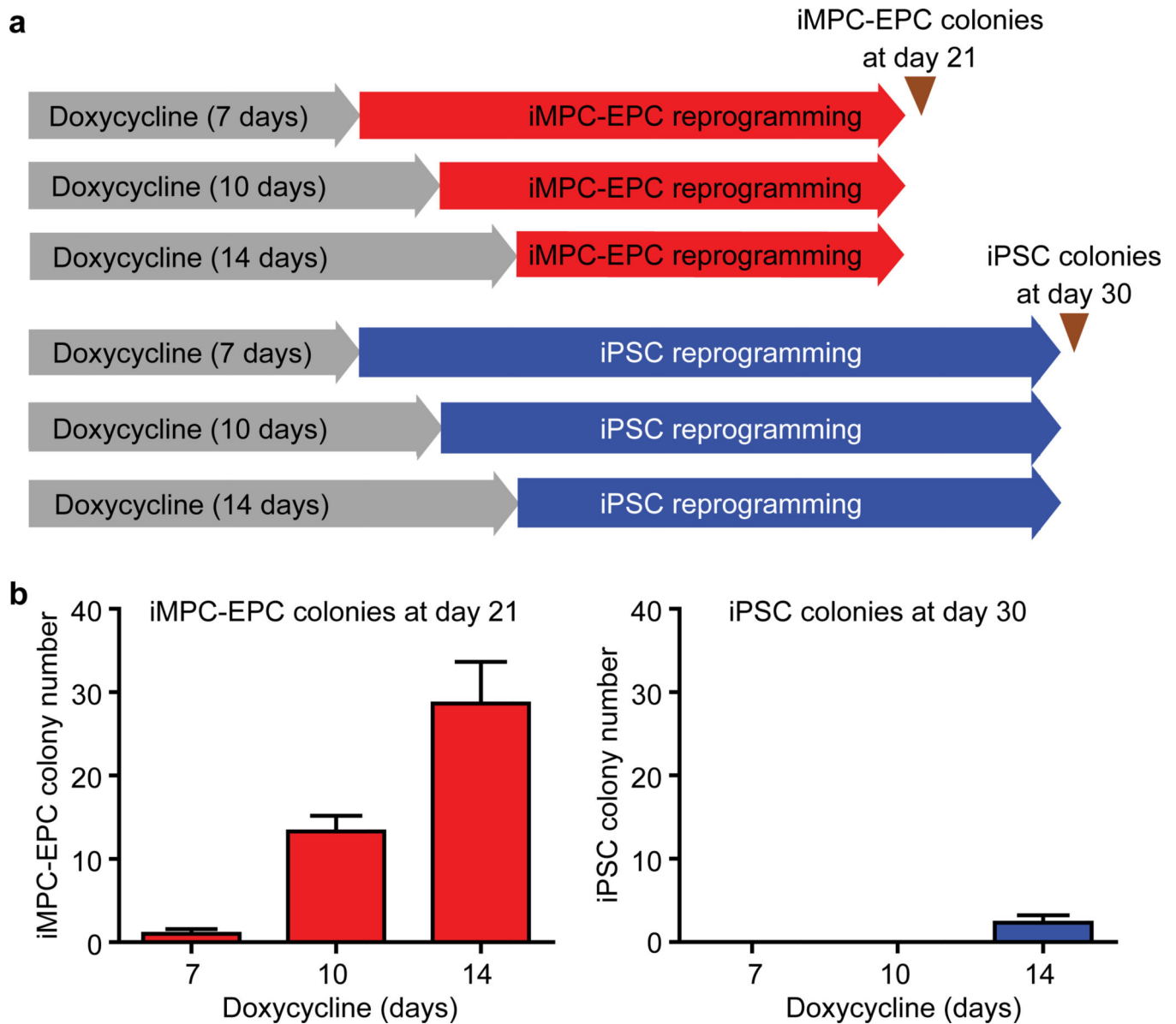
Extended Data Figure 3. Reprogramming of Fibs into iMPC-EPCs occurs earlier and is more efficient than reprogramming into iPSCs
a, Schematic showing duration of Dox treatment and time allowed for reprogramming to occur until analysis. **b,** Quantification of iMPC-EPC and iPSC colonies forming from Fibs cultured under iMPC-EPC and iPSC reprogramming conditions, respectively, in response to different durations of Dox treatment. iMPC-EPC and iPSC colonies were identified by FOXA2 and NANOG immunostaining, respectively. Error bars represent SEM of biological replicates (n = 3).
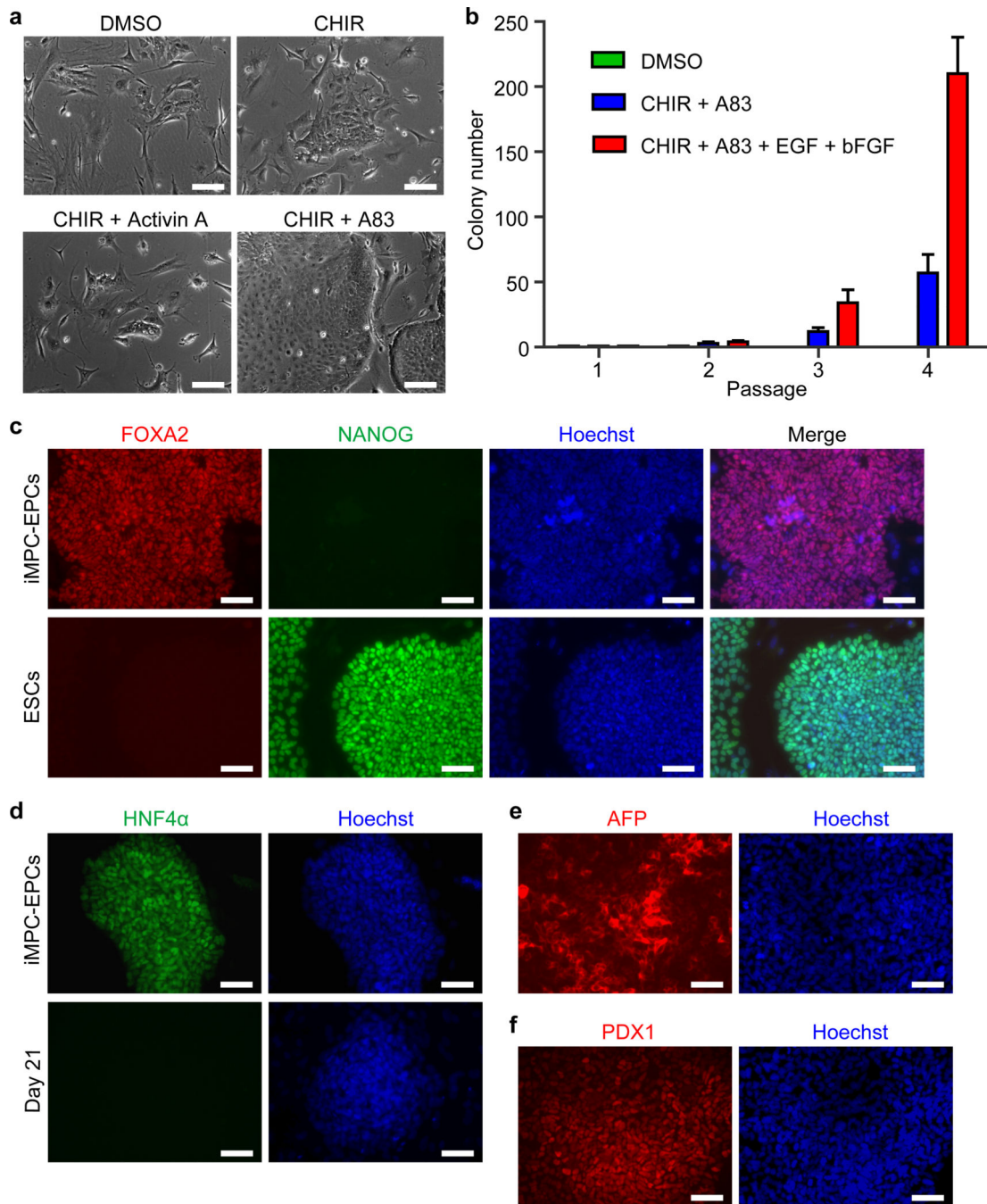
Extended Data Figure 4. Expansion and further characterization of iMPC-EPCs

a, Medium containing both CHIR and A83 promotes iMPC-EPC colony expansion. Scale bars = 100 μm. **b,** Supplementing medium containing both CHIR and A83 with EGF and bFGF further increases the number of iMPC-EPC colonies forming after passaging. Error bars represent SEM of biological replicates (n = 3). **c,** Immunostainings show that expanded (passage 7) iMPC-EPCs remain positive for FOXA2 and negative for NANOG. ESCs were used as controls. Scale bars = 100 μm. **d,** Immunostainings show HNF4α expression in an iMPC-EPC colony after expansion (passage 4), but not at day 21 of the reprogramming

process, indicating that expansion induces HNF4α expression. Scale bars = 100 μm. **e,** Immunostaining shows that iMPC-EPCs acquire expression of the hepatic differentiation marker AFP after exposure to bFGF and BMP4 for 4 days. **f,** Immunostaining shows that iMPC-EPCs acquire expression of the pancreatic differentiation marker PDX1 after exposure to retinoic acid, GDC-0449 (Sonic Hedgehog inhibitor), and LDN-193189 (BMP inhibitor) for 4 days. Scale bars = 100 μm.
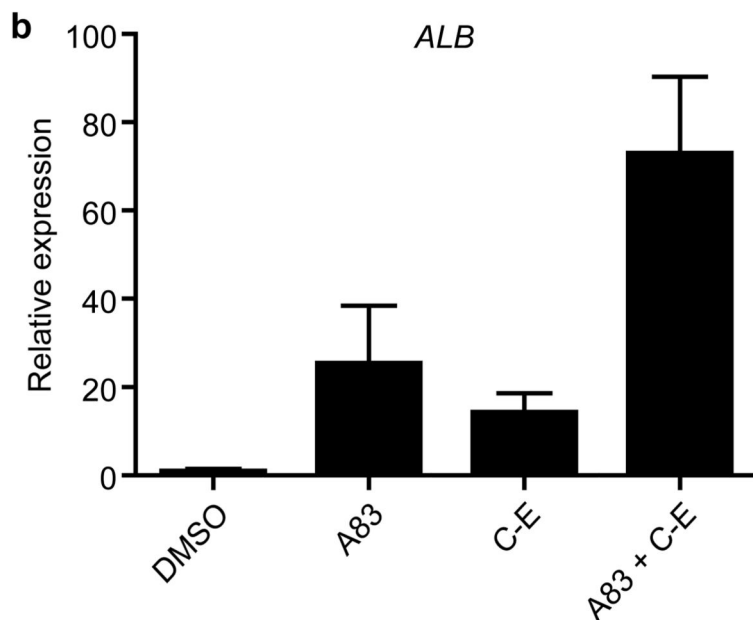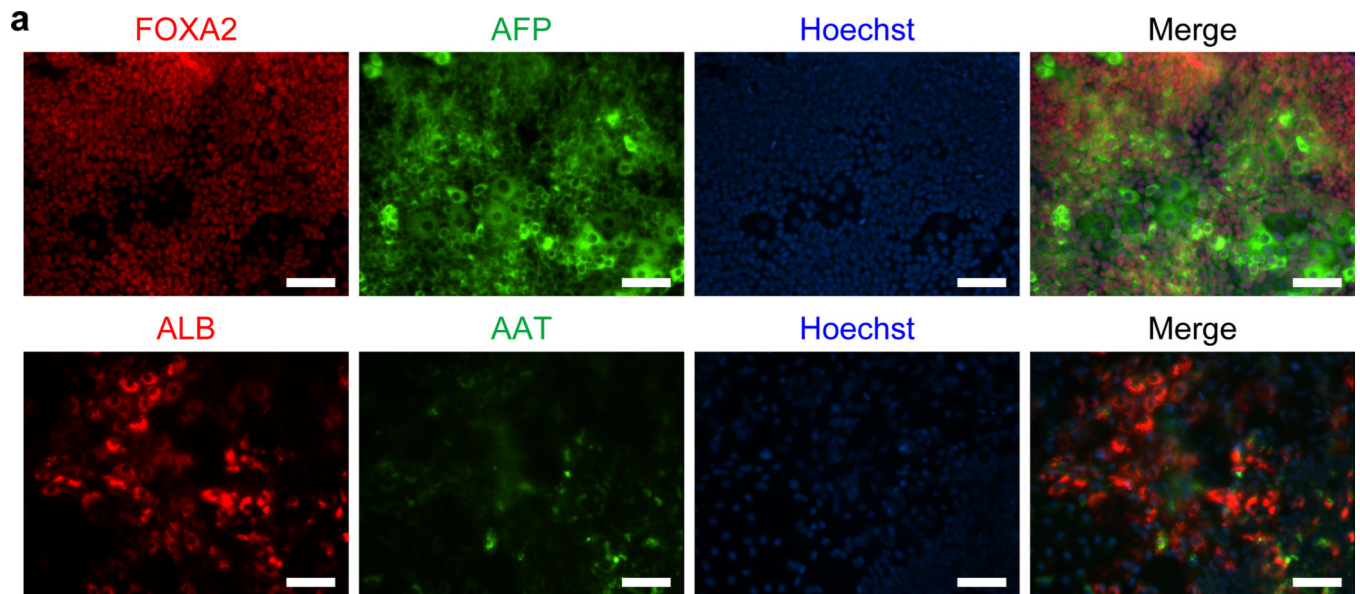
Extended Data Figure 5. Directed differentiation of iMPC-EPCs into iMPC-Heps
a, Immunostainings show that almost all iMPC-EPCs express AFP after sequential exposure to bFGF, BMP4, Dex, HGF, and OSM, whereas only a subset of the cells acquires ALB and AAT expression. Scale bars = 100 μm. **b,** qRT-PCR at day 18 of the hepatocyte

specification step of the protocol shows an additive effect of A83 and C-E in inducing expression of *ALB*. Gene expression levels are shown relative to iMPC-EPCs treated with carrier DMSO. Error bars represent SEM of technical replicates (n = 3).
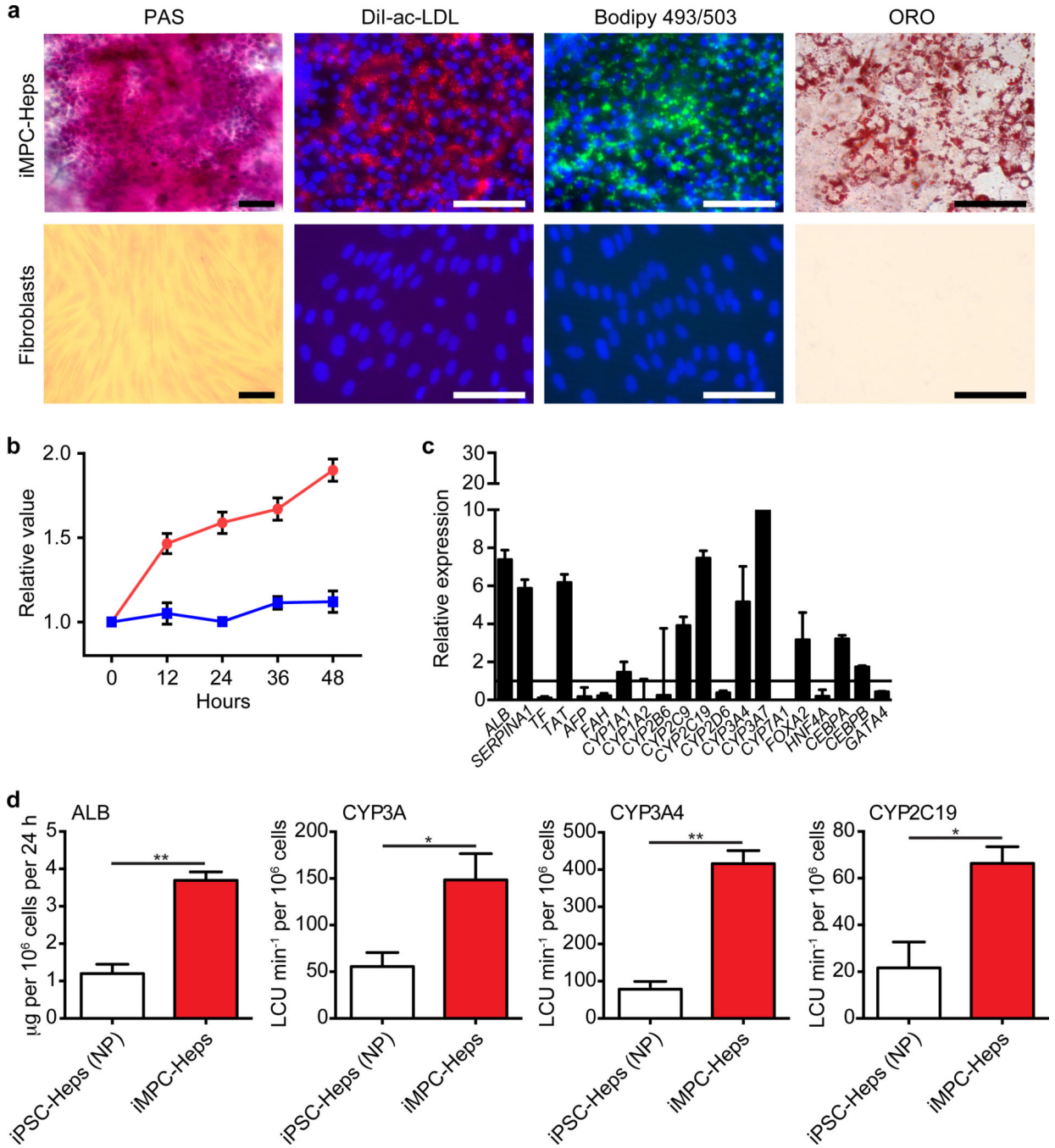
Extended Data Figure 6. Analysis of hepatocyte function of iMPC-Heps *in vitro*
a, Periodic acid-Schiff (PAS) staining shows that iMPC-Heps contain glycogen. Adding Dil-ac-low-density lipoprotein (LDL) fluorescent substrate to the culture medium shows that iMPC-Heps take up LDL. Incubation with BODIPY 493/503 or staining with Oil-red-O

(ORO) shows storage of lipids in iMPC-Heps. Fibs were used as negative controls. Scale bars = 100 μm. **b,** iMPC-Heps produce urea. The concentrations of urea measured in cell culture medium at the indicated time points are shown relative to the concentrations of urea measured in fresh medium. Fibs were used as negative control. Error bars represent SEM of biological replicates (n = 3). **c,** qRT-PCR shows higher expression of several hepatocyte-specific genes including *ALB* and *SERPINA1*, and lower expression of *AFP*, a marker of immature hepatocytes, in iMPC-Heps than in iPSC-Heps generated using current standard protocols. Gene expression of many CYP450 enzymes is also higher in iMPC-Heps than in iPSC-Heps, indicating that iMPC-Heps have a more mature hepatocyte phenotype than iPSC-Heps. Gene expression levels in iPSC-Heps were set to 1. Error bars represent SEM of technical replicates (n = 3). **d,** iMPC-Heps secrete more ALB and have higher CYP3A family, CYP3A4, and CYP2C19 activities than iPSC-Heps generated with the iMPC-EPC/Hep generation protocol, referred to as iPSC-Heps (NP). Results were calculated as the mean of biological replicates (n = 3). Error bars represent analytical SEM, *t* test, *$P < 0.05$, **$P < 0.01$.
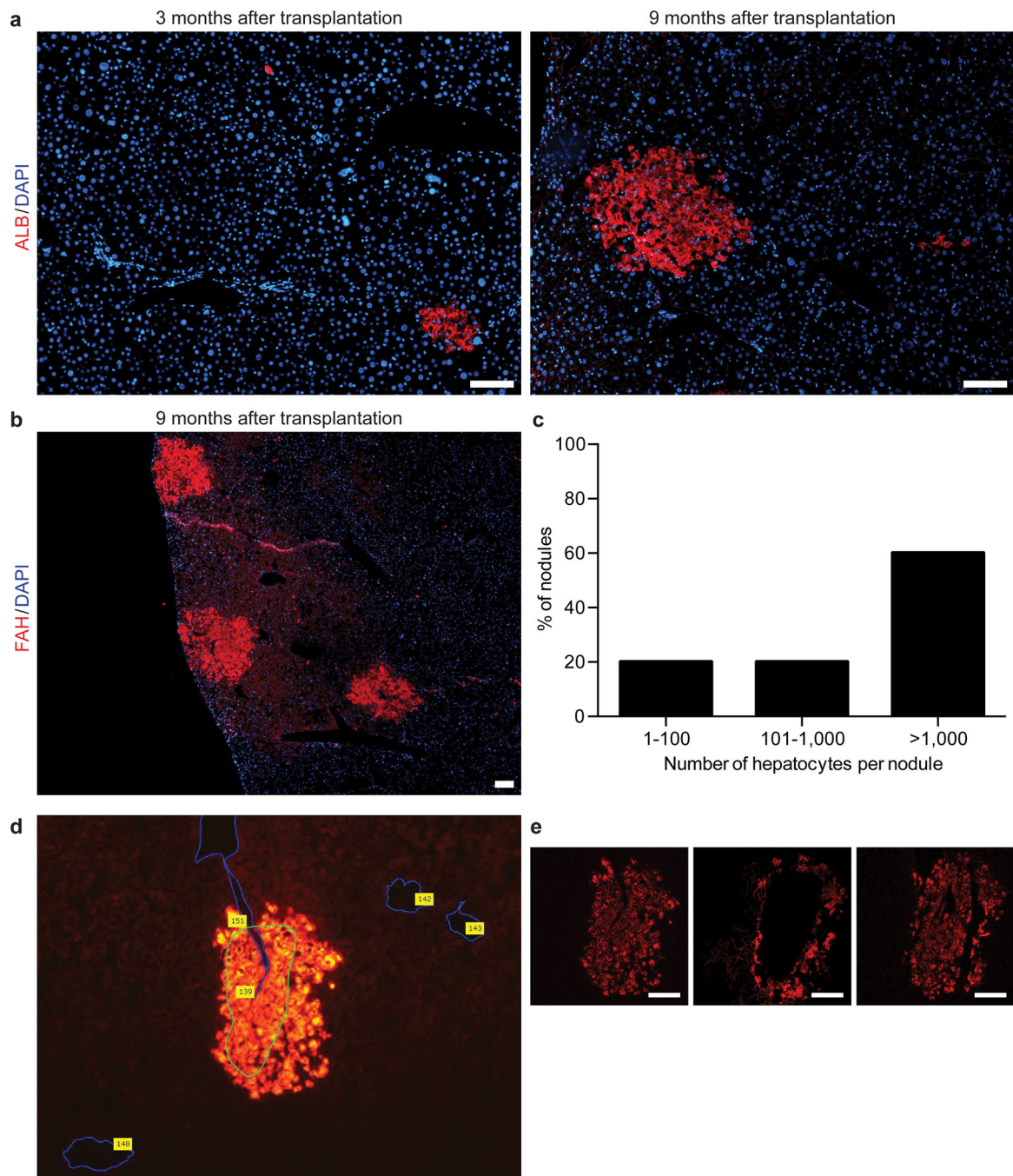
Extended Data Figure 7. Quantification and isolation of repopulating nodules formed by transplanted iMPC-Heps

a, Immunostainings show a small and a large nodule of iMPC-Heps detected with a human-specific ALB antibody at 3 and 9 months after transplantation. Scale bars = 100 μm. **b,** Multiple large nodules of iMPC-Heps identified by FAH immunostaining at 9 months after transplantation. Scale bar = 100 μm. **c,** Size distribution of nodules of iMPC-Heps 9 months after transplantation based on ALB and FAH immunostaining. **d,** Example of an iMPC-Hep nodule identified by ALB immunostaining for isolation by LCM. Blood vessels (numbers)

were used as additional markers of the location of a nodule in an adjacent, unfixed cryosection. **e,** Confirmation of successful isolation of an iMPC-Hep nodule by ALB immunostaining after LCM. The middle image shows a cryosection fixed and immunostained for ALB after LCM to confirm specific isolation of a nodule. The left and right images show ALB immunostainings of cryosections flanking the cryosection used for LCM. Scale bars = 100 μm.
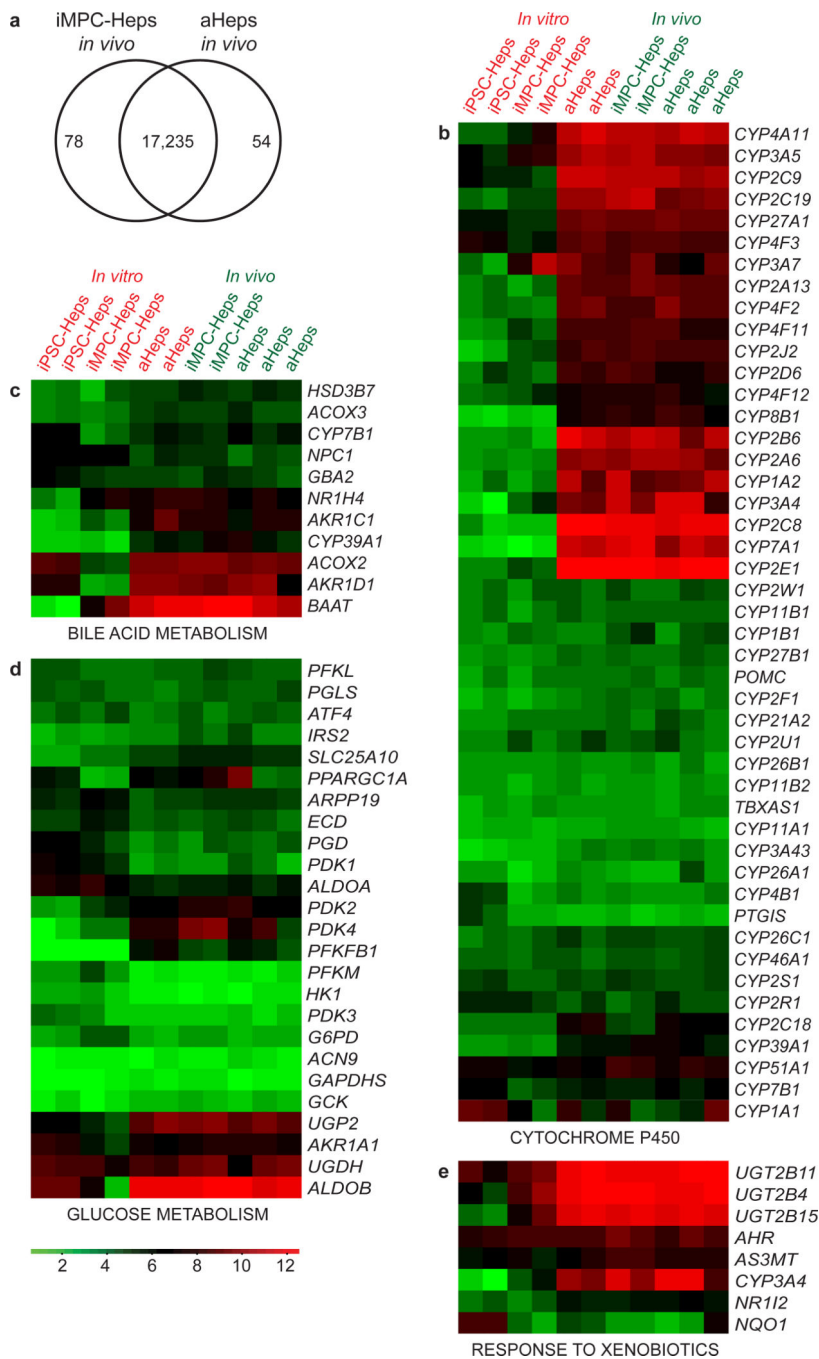

Extended Data Figure 8. Assessment of *in vivo* maturation of iMPC-Heps by global gene expression profiling

a, Venn diagram showing the number of genes significantly ($P < 0.05$) differentially expressed between iMPC-Heps and aHeps *in vivo*. Of 17,367 reliably detected genes, 132 are differentially expressed; 78 genes are expressed higher in iMPC-Heps and 54 genes are expressed higher in aHeps. The complete results of the global gene expression profiling—including the genes that are differentially expressed between aHeps and iMPC-Heps *in vivo*—are shown in Supplementary Table 2. **b-e,** Further analysis of results from global gene expression profiling using gene sets of the hepatocyte function-related Gene Ontology (GO) terms REACTOME CYTOCHROME P450 ARRANGED BY SUBSTRATE TYPE (**b**), BILE ACID METABOLIC PROCESS (**c**), GLUCOSE METABOLIC PROCESS (**d**), and RESPONSE TO XENOBIOTIC STIMULUS (**e**). GO terms and annotated genes were obtained from Molecular Signatures Database (MSigDB) v4.0. Heatmaps were generated individually for each GO term; a representative colour legend is shown. All results are from one microarray analysis.
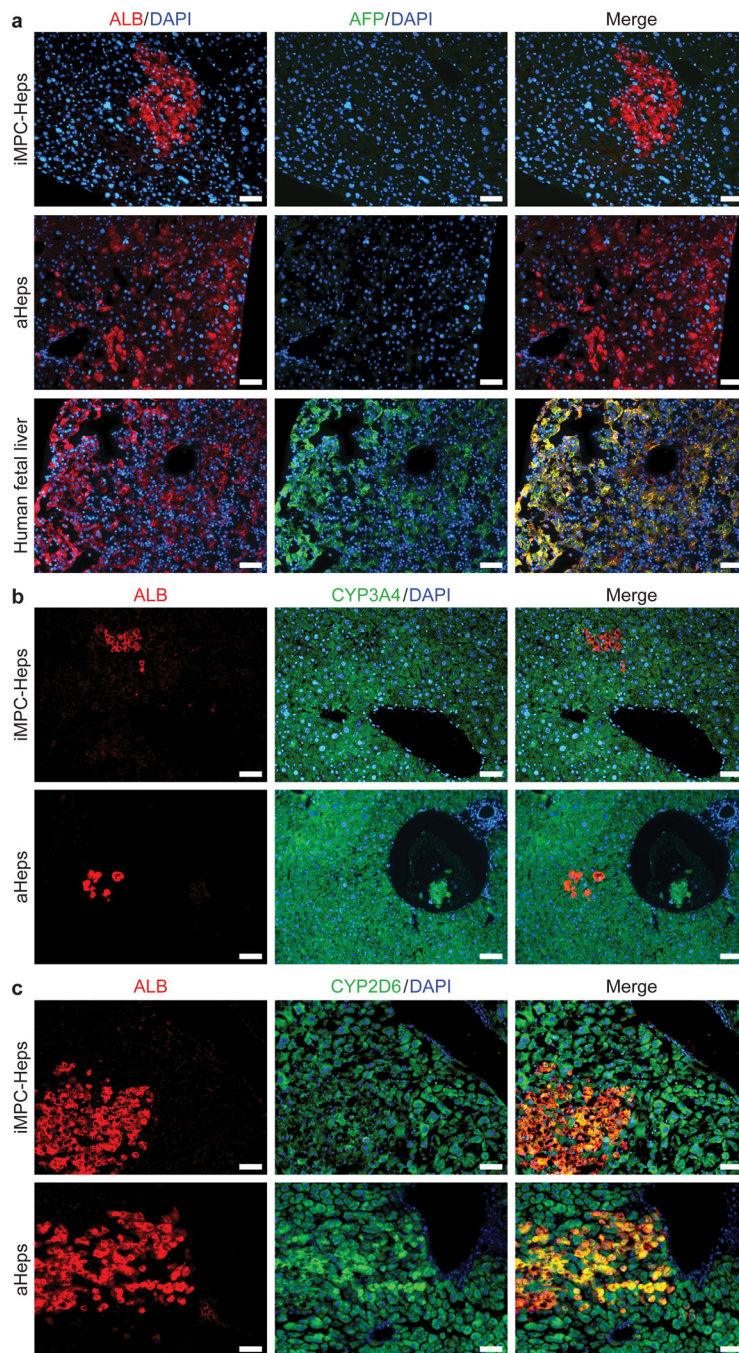
Extended Data Figure 9. Assessment of *in vivo* maturation of iMPC-Heps by immunostaining
a, Co-immunostaining for ALB and AFP shows lack of expression of the immature hepatocyte-specific marker AFP in iMPC-Hep and aHep nodules. Human fetal liver was used as a positive control. Scale bars = 100 μm. **b,c,** Co-immunostainings for ALB and CYP3A4 (**b**) or CYP2D6 (**c**) show expression of these mature hepatocyte-specific markers in iMPC-Heps. Of note, the CYP450 antibodies detect the mouse homologues of CYP3A4 and CYP2D6, which—as in humans—appear to be expressed in hepatocytes, but not in nonparenchymal liver cells. Scale bars = 100 μm.
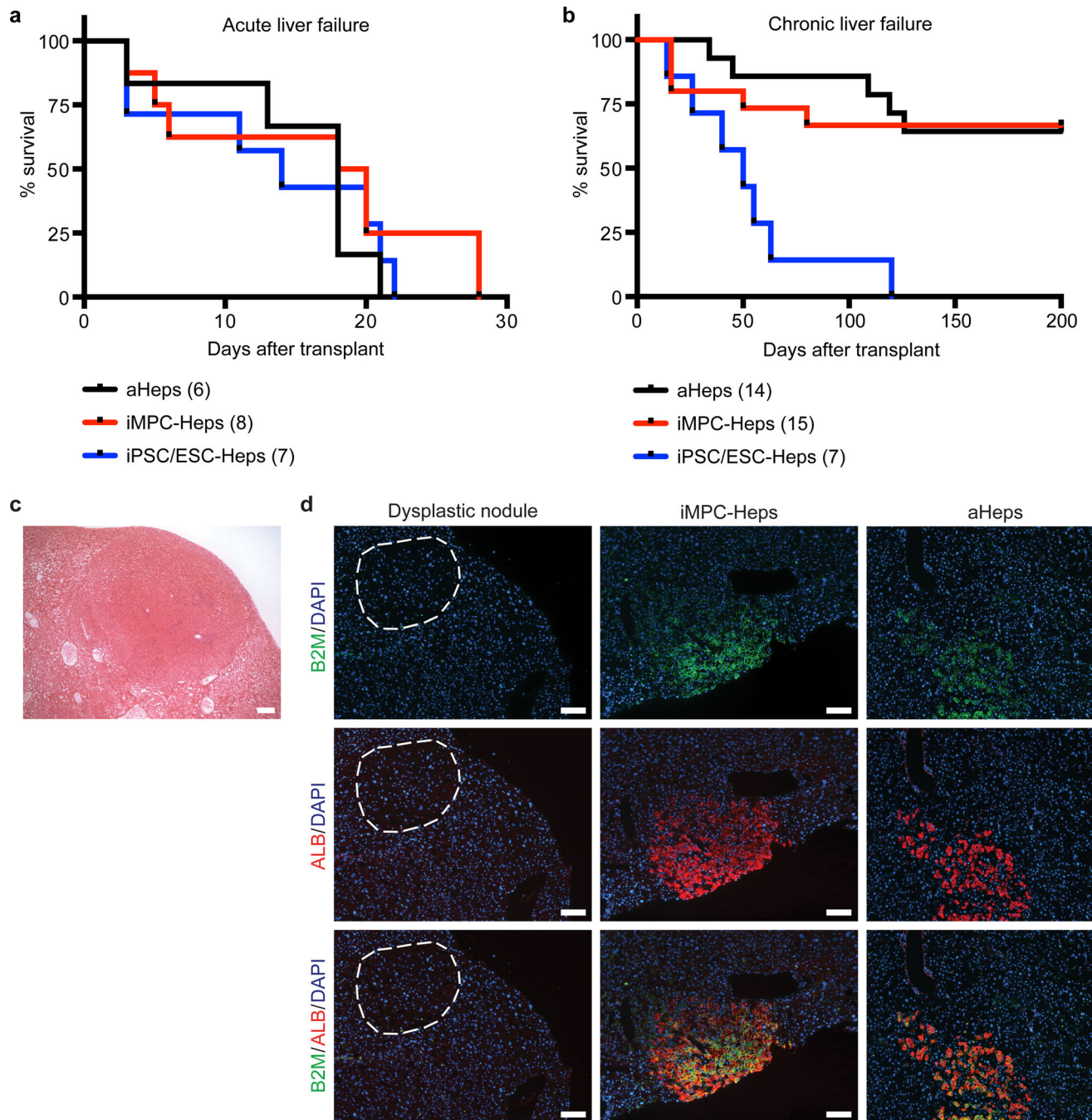
Extended Data Figure 10. Therapeutic efficacy and safety of iMPC-Heps
a, Kaplan-Meier survival curve shows that 1×10^6 transplanted iMPC-Heps, iPSC/ESC-Heps, or aHeps are not effective in rescuing mice from death from acute liver failure. Log-rank test $P = 0.4426$ between iMPC-Heps and iPSC/ESC-Heps, $P = 0.4031$ between iMPC-Heps and aHeps. **b,** Kaplan-Meier survival curve shows similar efficacy of 1×10^6 transplanted aHeps and iMPC-Heps, but not iPSC/ESC-Heps, in preventing death in mice suffering from chronic liver failure. Log-rank test $P < 0.01$ between iMPC-Heps and iPSC/ESC-Heps, $P = 0.9501$ between iMPC-Heps and aHeps. The number of mice in each group

is shown in parentheses. **c,** H&E staining shows a dysplastic nodule in the liver of an FRG mouse transplanted with iMPC-Heps. Scale bar = 100 μm. **d,** Co-immunostaining with human-specific β2-microglobulin (B2M) and ALB antibodies shows that the cells within dysplastic nodules (dashed line) are negative for both markers and therefore of mouse origin. Scale bars = 100 μm. Nodules of iMPC-Heps or aHeps are shown as controls.

Supplementary Material

Refer to Web version on PubMed Central for supplementary material.

ACKNOWLEDGEMENTS

REFERENCES

1. Si-Tayeb K, et al. Highly efficient generation of human hepatocyte-like cells from induced pluripotent stem cells. Hepatology. 2010; 51:297–305. [PubMed: 19998274]

2. Rashid ST, et al. Modeling inherited metabolic disorders of the liver using human induced pluripotent stem cells. J Clin Invest. 2010; 120:3127–3136. [PubMed: 20739751]

3. Ma X, et al. Highly efficient differentiation of functional hepatocytes from human induced pluripotent stem cells. Stem Cells Transl Med. 2013; 2:409–419. [PubMed: 23681950]

4. Puppi J, et al. Improving the techniques for human hepatocyte transplantation: report from a consensus meeting in London. Cell Transplant. 2012; 21:1–10. [PubMed: 21457616]

5. Liu H, Kim Y, Sharkis S, Marchionni L, Jang YY. In vivo liver regeneration potential of human induced pluripotent stem cells from diverse origins. Sci Transl Med. 2011; 3:82ra39.

6. Basma H, et al. Differentiation and transplantation of human embryonic stem cell-derived hepatocytes. Gastroenterology. 2009; 136:990–999. [PubMed: 19026649]

7. Woo DH, et al. Direct and indirect contribution of human embryonic stem cell-derived hepatocyte-like cells to liver repair in mice. Gastroenterology. 2012; 142:602–611. [PubMed: 22138358]

8. Azuma H, et al. Robust expansion of human hepatocytes in Fah−/−/Rag2−/−/Il2rg−/− mice. Nat Biotechnol. 2007; 25:903–910. [PubMed: 17664939]

9. Szabo E, et al. Direct conversion of human fibroblasts to multilineage blood progenitors. Nature. 2010; 468:521–526. [PubMed: 21057492]

10. Kurian L, et al. Conversion of human fibroblasts to angioblast-like progenitor cells. Nat Methods. 2013; 10:77–83. [PubMed: 23202434]

11. Li J, et al. Conversion of human fibroblasts to functional endothelial cells by defined factors. Arterioscler Thromb Vasc Biol. 2013; 33:1366–1375. [PubMed: 23520160]

12. Takahashi K, et al. Induction of pluripotent stem cells from adult human fibroblasts by defined factors. Cell. 2007; 131:861–872. [PubMed: 18035408]

13. Zhu S, et al. Reprogramming of human primary somatic cells by OCT4 and chemical compounds. Cell Stem Cell. 2010; 7:651–655. [PubMed: 21112560]

14. Lee JM, et al. A nuclear-receptor-dependent phosphatidylcholine pathway with antidiabetic effects. Nature. 2011; 474:506–510. [PubMed: 21614002]

15. Chan EM, et al. Live cell imaging distinguishes bona fide human iPS cells from partially reprogrammed cells. Nat Biotechnol. 2009; 27:1033–1037. [PubMed: 19826408]

16. Li W, et al. Rapid induction and long-term self-renewal of primitive neural precursors from human embryonic stem cells by small molecule inhibitors. Proc Natl Acad Sci U S A. 2011; 108:8299–8304. [PubMed: 21525408]

17. Wang P, Rodriguez RT, Wang J, Ghodasara A, Kim SK. Targeting SOX17 in human embryonic stem cells creates unique strategies for isolating and analyzing developing endoderm. Cell Stem Cell. 2011; 8:335–346. [PubMed: 21362573]

18. Cheng X, et al. Self-renewing endodermal progenitor lines generated from human pluripotent stem cells. Cell Stem Cell. 2012; 10:371–384. [PubMed: 22482503]

19. Clotman F, et al. Control of liver cell fate decision by a gradient of TGF beta signaling modulated by Onecut transcription factors. Genes Dev. 2005; 19:1849–1854. [PubMed: 16103213]

20. Kodama Y, Hijikata M, Kageyama R, Shimotohno K, Chiba T. The role of notch signaling in the development of intrahepatic bile ducts. Gastroenterology. 2004; 127:1775–1786. [PubMed: 15578515]

21. Chen AA, et al. Humanized mice with ectopic artificial liver tissues. Proc Natl Acad Sci U S A. 2011; 108:11842–11847. [PubMed: 21746904]

22. Kroon E, et al. Pancreatic endoderm derived from human embryonic stem cells generates glucose-responsive insulin-secreting cells in vivo. Nat Biotechnol. 2008; 26:443–452. [PubMed: 18288110]

23. Willenbring H, et al. Loss of p21 permits carcinogenesis from chronically damaged liver and kidney epithelial cells despite unchecked apoptosis. Cancer Cell. 2008; 14:59–67. [PubMed: 18598944]

24. Lin T, et al. A chemical platform for improved induction of human iPSCs. Nat Methods. 2009; 6:805–808. [PubMed: 19838168]

25. Song Z, et al. Efficient generation of hepatocyte-like cells from human induced pluripotent stem cells. Cell Res. 2009; 19:1233–1242. [PubMed: 19736565]

26. Maherali N, et al. A high-efficiency system for the generation and study of human induced pluripotent stem cells. Cell Stem Cell. 2008; 3:340–345. [PubMed: 18786420]

27. Andreou ER, Prokipcak RD. Analysis of human CYP7A1 mRNA decay in HepG2 cells by reverse transcription-polymerase chain reaction. Arch Biochem Biophys. 1998; 357:137–146. [PubMed: 9721193]

28. Leeder JS, et al. Variability of CYP3A7 expression in human fetal liver. J Pharmacol Exp Ther. 2005; 314:626–635. [PubMed: 15845858]

29. Zhang X, Ding L, Sandford AJ. Selection of reference genes for gene expression studies in human neutrophils by real-time PCR. BMC Mol Biol. 2005; 6:4. [PubMed: 15720708]

30. Aninat C, et al. Expression of cytochromes P450, conjugating enzymes and nuclear receptors in human hepatoma HepaRG cells. Drug Metab Dispos. 2006; 34:75–83. [PubMed: 16204462]

31. Martinez-Jimenez CP, Castell JV, Gomez-Lechon MJ, Jover R. Transcriptional activation of CYP2C9, CYP1A1, and CYP1A2 by hepatocyte nuclear factor 4alpha requires coactivators peroxisomal proliferator activated receptor-gamma coactivator 1alpha and steroid receptor coactivator 1. Mol Pharmacol. 2006; 70:1681–1692. [PubMed: 16882880]

32. Xie CQ, et al. Expression profiling of nuclear receptors in human and mouse embryonic stem cells. Mol Endocrinol. 2009; 23:724–733. [PubMed: 19196830]

33. Mwinyi J, et al. Regulation of CYP2C19 expression by estrogen receptor alpha: implications for estrogen-dependent inhibition of drug metabolism. Mol Pharmacol. 2010; 78:886–894. [PubMed: 20675569]

34. Lieber A, et al. Adenovirus-mediated urokinase gene transfer induces liver regeneration and allows for efficient retrovirus transduction of hepatocytes in vivo. Proc Natl Acad Sci U S A. 1995; 92:6210–6214. [PubMed: 7597103]

35. Espejel S, et al. Induced pluripotent stem cell-derived hepatocytes have the functional and proliferative capabilities needed for liver regeneration in mice. J Clin Invest. 2010; 120:3120–3126. [PubMed: 20739754]

36. Hasegawa M, et al. The reconstituted 'humanized liver' in TK-NOG mice is mature and functional. Biochem Biophys Res Commun. 2011; 405:405–410. [PubMed: 21238430]

37. Wang X, et al. Kinetics of liver repopulation after bone marrow transplantation. Am J Pathol. 2002; 161:565–574. [PubMed: 12163381]
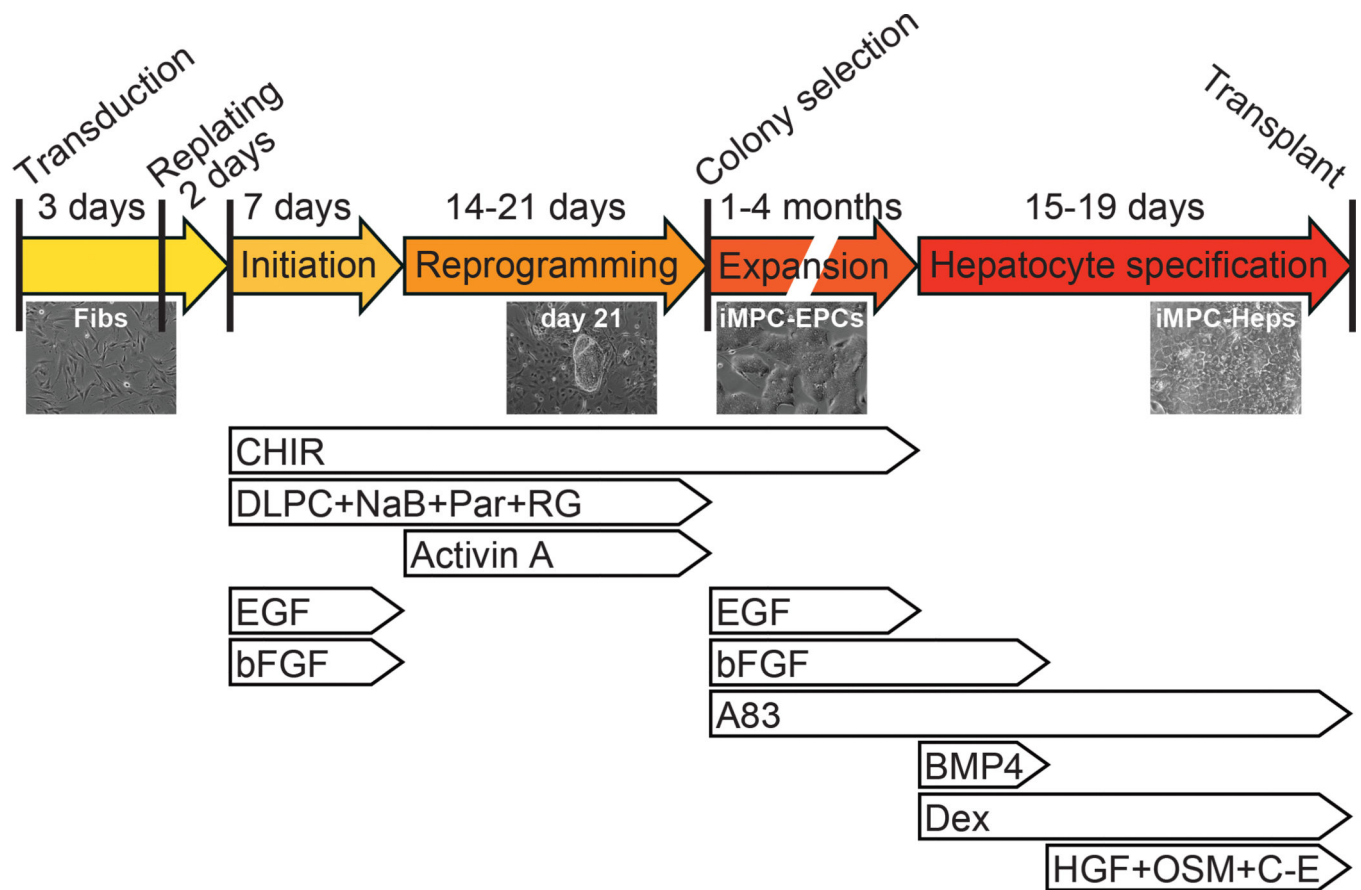
Figure 1. Protocol for stepwise iMPC-Hep generation

Reprogramming of Fibs to endoderm was initiated in medium containing CHIR (GSK3β inhibitor), dilauroyl phosphatidylcholine (DLPC; LRH1 agonist), the epigenetic modifiers sodium butyrate (NaB; HDAC inhibitor), Parnate (Par; LSD1 inhibitor), and RG108 (RG; DNMT inhibitor), and epidermal growth factor (EGF) and basic fibroblast growth factor (bFGF). To promote reprogramming, EGF and bFGF were replaced with Activin A. Individual iMPC-EPC colonies were expanded in medium containing CHIR, EGF, bFGF, and A83 (TGFβ type I receptor inhibitor). For hepatocyte specification, medium containing bFGF, A83, bone morphogenetic protein 4 (BMP4), dexamethasone (Dex), hepatocyte growth factor (HGF), oncostatin M (OSM), and C–E was used.
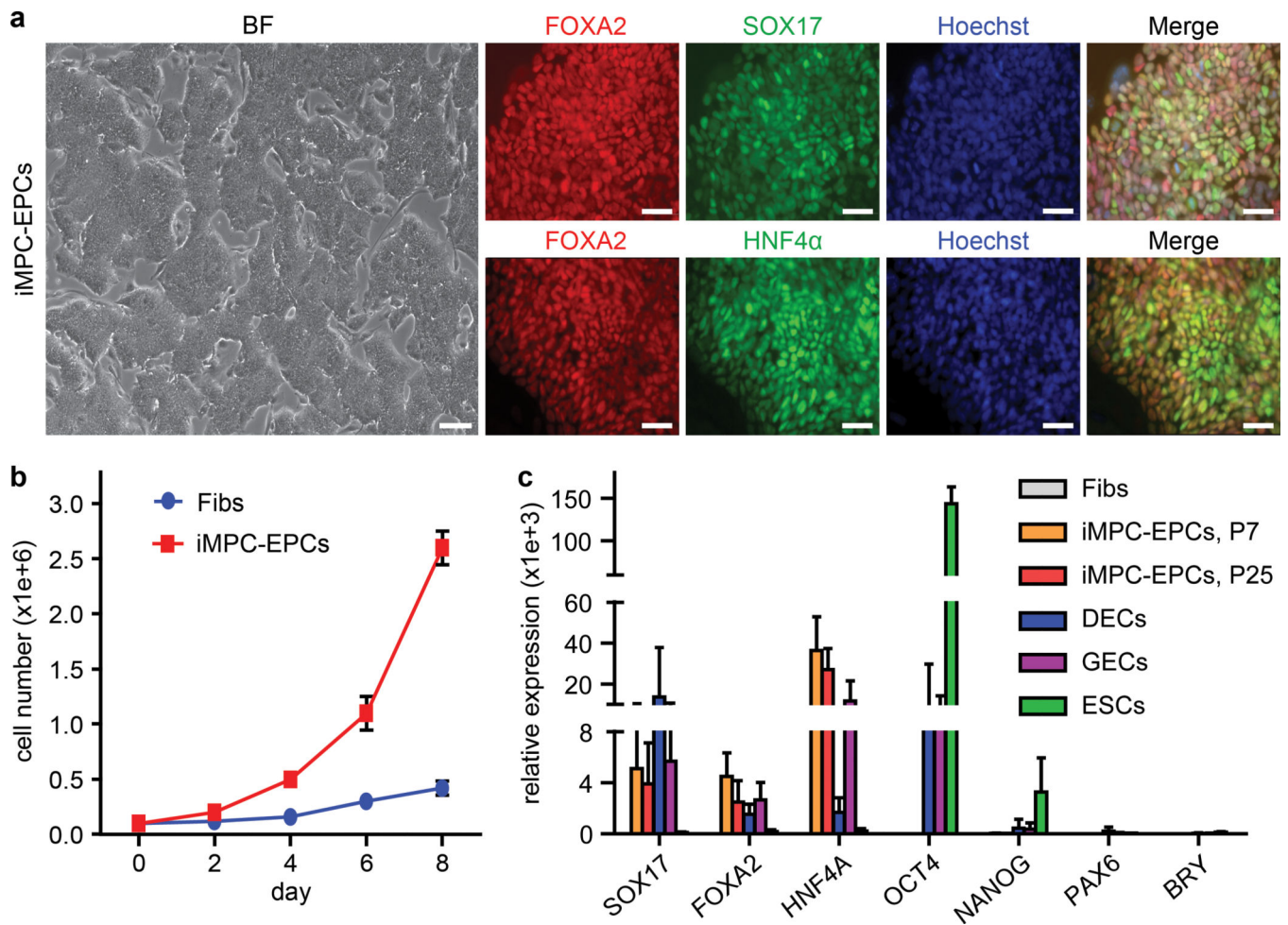
Figure 2. Characterization of iMPC-EPCs

a, Bright field (BF) microscopy shows morphology of iMPC-EPCs at passage 25; immunostainings show expression of FOXA2, SOX17, and HNF4α. Scale bars = 100 μm. **b**, Expansion capacity of iMPC-EPCs as compared to Fibs. Cell numbers were counted at indicated time points. Error bars represent SEM of biological replicates (n = 3). **c**, qRT-PCR of genes specific for endoderm, pluripotency, ectoderm, or mesoderm in iMPC-EPCs as compared to Fibs, ESCs, and ESC-derived DECs or GECs. Gene expression levels are shown relative to Fibs. Error bars represent SEM of technical replicates (n = 3).
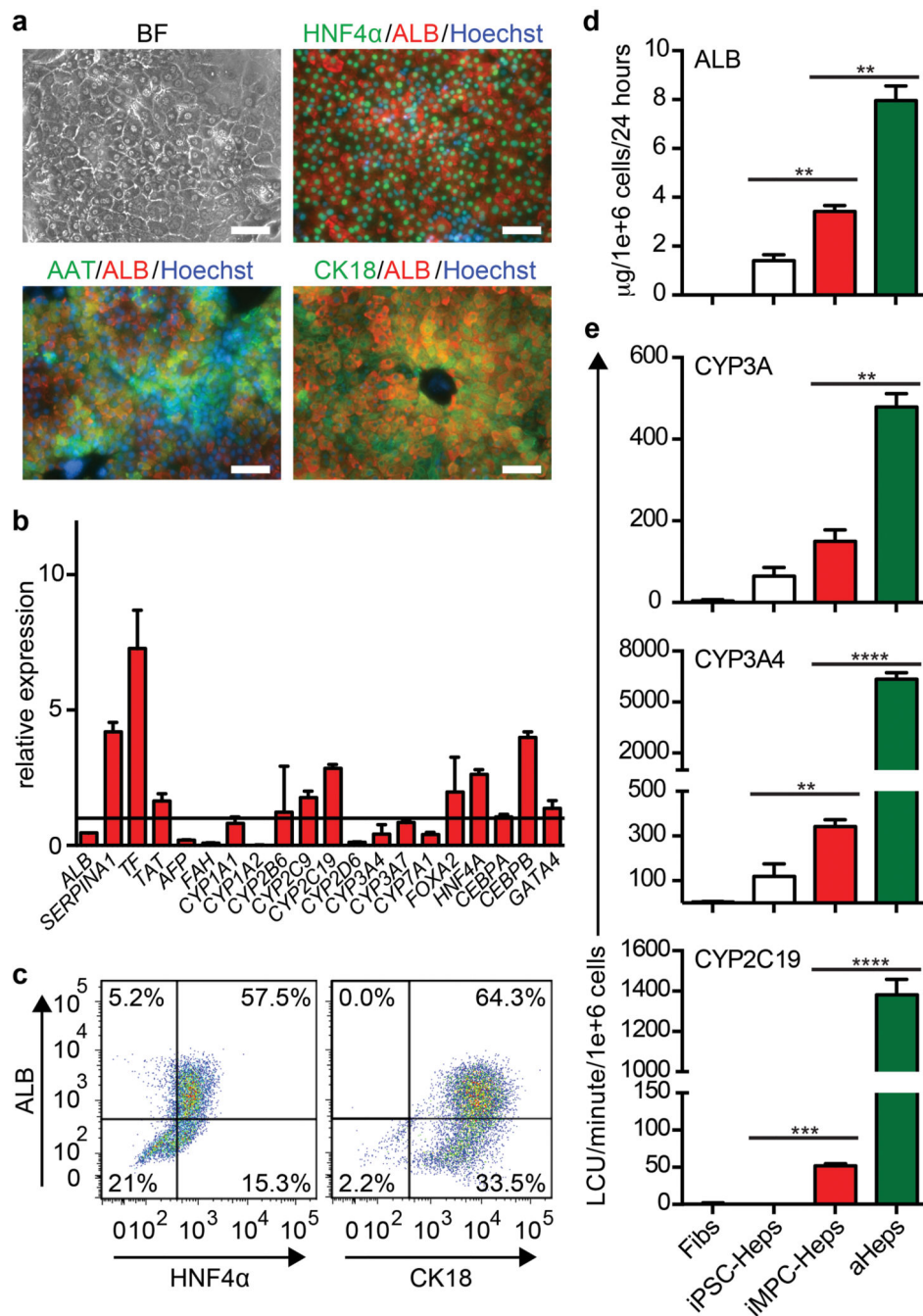
Figure 3. Characterization of iMPC-Heps

a, BF microscopy shows morphology of iMPC-Heps; immunostainings show expression of HNF4α, ALB, AAT, and CK18. Scale bars = 100 μm. **b**, qRT-PCR of hepatocyte marker gene expression in iMPC-Heps relative to fHeps. The immature hepatocyte-specific genes *CYP1A1/3A7* and the mature hepatocyte-specific genes *CYP2B6/2C9/2C19/3A4*, but not *CYP1A2/2D6*, are expressed at similar levels in iMPC-Heps and fHeps. Error bars represent SEM of technical replicates (n = 3). **c**, Flow cytometry shows that most iMPC-Heps express ALB, HNF4α, and CK18. **d**, Enzyme-linked immunosorbent assay (ELISA) shows

significant ALB secretion by iMPC-Heps as compared to Fibs, iPSC-Heps, and aHeps. Error bars represent SEM of biological replicates (n = 3), *t* test, **P < 0.01. **e**, Quantification of the activities of the CYP3A family (assay selectivity: CYP3A5   CYP3A5 > CYP3A4), CYP3A4, and CYP2C19 shows higher levels in iMPC-Heps than in iPSC-Heps. Fibs and aHeps were used as negative and positive controls, respectively. Error bars represent SEM of biological replicates (n = 3), *t* test, **P < 0.01, ***P < 0.001, ****P < 0.0001.
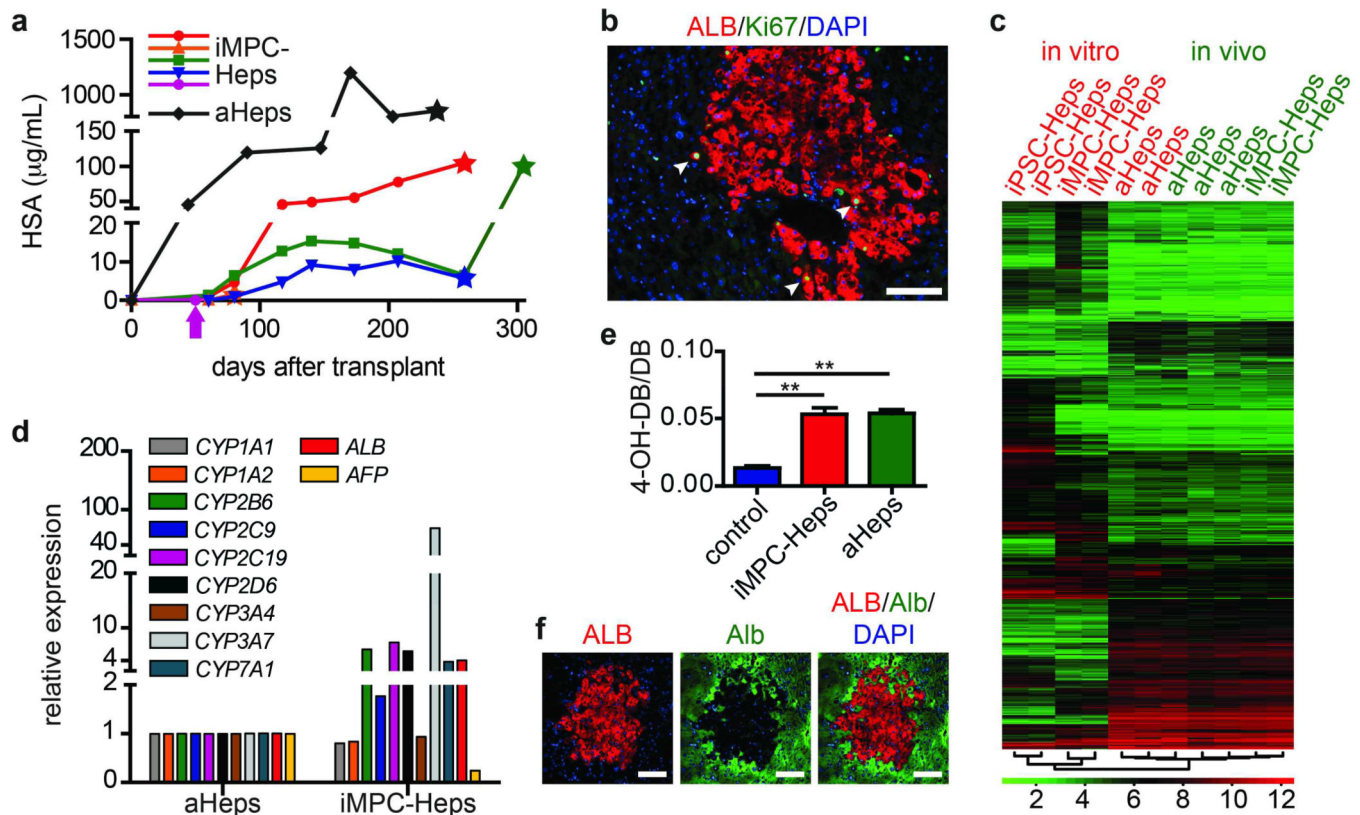
Figure 4. Post-transplant proliferation and maturation of iMPC-Heps

a, HSA levels in recipients of iMPC-Heps or aHeps. Stars indicate time points of analysis. Arrow marks fatality. **b**, Co-immunostaining for human-specific ALB and Ki67 identifies proliferating iMPC-Heps (arrowheads) in the periphery of a repopulating nodule. Scale bar = 100 μm. **c**, Heatmap of 1,299 genes differentially expressed between iMPC-Heps, freshly isolated aHeps and iPSC-Heps before (*in vitro*) and after (*in vivo*) transplantation. Multiple nodules were pooled to generate a sample. Genes with expression levels below background (log2 normalized expression < 3) and genes not varying over all samples (s.d. expression < 1) were filtered out. Hierarchical clustering was performed with the hclust function in R v. 2.15.1. **d**, qRT–PCR of the samples used for microarray analysis shows mean hepatocyte marker gene expression in iMPC-Heps relative to aHeps *in vivo*. **e**, Analysis of human-specific CYP2D6-mediated DB metabolism in iMPC-Hep- or aHep-repopulated mice by liquid chromatography-tandem mass spectrometry (LC-MS/MS). Plasma levels of DB and its metabolite 4-OH-DB peaked 1 hour after gavage. Molar 4-OH-DB/DB ratios at 1 hour are shown, calculated as the mean of the ratios for repeat injections (n = 3). Error bars represent analytical SEM, *t* test, **$P < 0.01$. **f**, Co-immunostaining with human-specific ALB and mouse-specific Alb antibodies shows absence of double-positive cells, which rules out fusion of iMPC-Heps with mouse hepatocytes. Scale bars = 100 μm.